UNIVERSITY OF OKLAHOMA

GRADUATE COLLEGE

INDUCED FRACTURE DETECTION IN THE BARNETT SHALE, FT. WORTH BASIN, TEXAS

A THESIS

SUBMITTED TO THE GRADUATE FACULTY

in partial fulfillment of the requirement for the

Degree of

MASTER OF SCIENCE

By

AMANDA MARIE THOMPSON
Norman, Oklahoma
2010

INDUCED FRACTURE DETECTION IN THE BARNETT SHALE, FT. WORTH BASIN, TEXAS

A THESIS APPROVED FOR THE
CONOCOPHILLIPS SCHOOL OF GEOLOGY AND GEOPHYSICS

BY

_____

Dr. Kurt Marfurt

_____

Dr. Heloise Lynn

_____

Dr. Katie Keranen

ACKNOWLEDGEMENTS

I cannot adequately express my gratitude to Mike Ammerman, for not only the completion of this thesis, but also the beginning, middle, and every minor detail in between. This seismic experiment was his last project as a full-time Devon employee and I am so thankful for having had the chance to work on it with him. Mike has been a wonderful role model to me and I am proud to have worked with him and represent this project.

The completion of this thesis would have not been possible without the guidance, support and contributions from everyone else involved in this project. First of all I would like to thank my committee members, my advisor, Dr. Kurt Marfurt; Dr. Heloise Lynn and Dr. Katie Keranen for their ongoing support, encouragement and expertise. I would also like to thank Devon Energy and Jeff Hall for the use of the data and permission to publish my findings. I am extremely grateful for the support everyone has extended to me while taking classes and working full time. I thank my family for all of their love and support throughout my school years. Finally, I would like to extend a huge thank you to Dr. Jamie Rich for his technical help and advice. He has also been a great facilitator of motivation and critical thinking for me this last year.

TABLE OF CONTENTS

LIST OF TABLES

LIST OF FIGURES

ABSTRACT

Production from the Barnett Shale requires hydraulic fracturing to provide pathways for fluid flow. Areas of pre-existing hydraulic fractures are typically avoided because of the potential interference with other wells in the area. Areas stimulated by hydraulically-induced fractures need to be mapped in order to effectively place and complete in-fill wells. Engineering data (EUR values) alone cannot predict the stimulated area. Seismic data has been proven useful in predicting natural fractures and mapping stimulated areas using traditional 4D experiments. In this study I will attempt to use 3D seismic data and engineering data to identify and map the hydraulically-induced fractures.

Although seismic data and its derivative products (attributes, velocity anisotropy, AVAz) have been used to map natural fractures, little has been reported on mapping induced fractures. I develop a workflow that uses 3D seismic data to extrapolate engineering data (EUR, fracability) from sparse well control to the dense seismic grid. My original objective was to use the rich collection of image logs and micro-seismic experiments to establish a relationship between engineering and production data, and 3D surface seismic measurements, thereby extending my workflow to areas where these 'specialty logs' have not been acquired. This was attempted but due to the heterogeneity of completion techniques, a correlation could not be reached with satisfactory results.

In contrast, prestack analysis shows a clear image of the fracture network established by the extensive hydraulic fracture effort. Although all 135 horizontal

wells were drilled NW-SE, perpendicular to the major NE-SW horizontal stress axis, the resulting P-wave anisotropy indicates highly compartmentalized anisotropy, with the anisotropy of the different compartments oriented in all azimuthal directions. Confirming this interpretation, P-wave anisotropy of the underlying Viola and overlying Marble Falls limestone fracture barriers are very homogeneous, trending in an ENE-WSW azimuth. Micro-seismic event locations show that these frac barriers were unaffected by the hydraulic fracture processes.

The results of these findings have two major implications. First, the fractures initiated by hydraulic fracturing do not all trend in the direction of the regional maximum horizontal stress. Rather, it appears that once a local fracture network has been established, the new stress regime controls subsequent hydraulically-induced fractures. Second, accurate maps of the local anisotropy can be used to guide the direction of wells used to produce by-passed pay or to modify future stimulation procedures in those parts of the reservoir that have already been fractured but are underperforming.

CHAPTER 1

INTRODUCTION

Currently natural gas supplies 22 percent of the United States' energy demands (Ground Water Protection Council, 2009). Over half of this production comes from unconventional reservoirs, with this component expected to grow in the coming years. Figure 1 shows the prediction of growth for unconventional reservoirs. Production from shale gas is emerging as one of the most important natural gas resources in North America. The Fort Worth Basin is currently the largest shale gas producer in the United States, contributing almost 4000 MMcf/day of the nearly 5000 MMcf/day total from six different shale-gas plays in 2008 (Ground Water Protection Council, 2009).

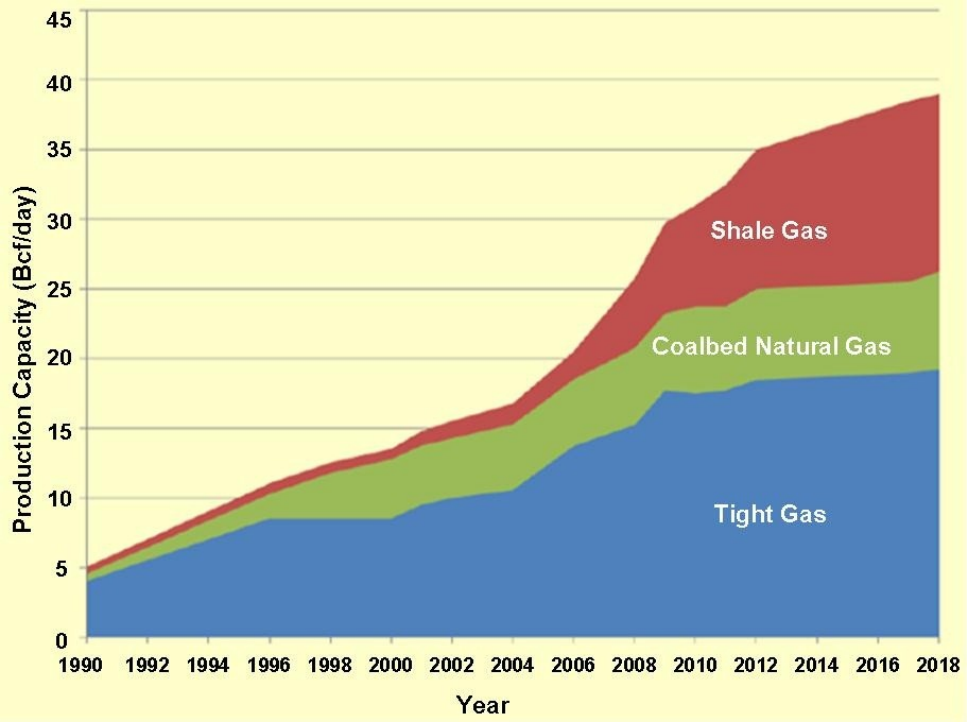

Figure 1. Prediction of growth in unconventional resource plays in the United States over the next 8 years. (After Ground Water Protection Council, 2009).

In the Ft. Worth Basin it is critical to artificially fracture the near-zero permeability reservoir in order to create high-performing gas wells. Recent technological developments in drilling and hydraulic stimulation, coupled with relatively high gas prices make the Barnett Shale economical. Due to the dense well control (over 10,000 wells in the basin) the target and thickness is known.

3D seismic data cover the basin and are used to map fault and fracture trends. These data are also used to map the thickness and location of fracture barriers and paleo zones of weakness in order to better guide and stimulate horizontal wells. Seismic images are also valuable in mapping connectivity of karsts to the underlying Ellenberger formation; such connectivity can be indicative of water production and should be avoided when drilling and stimulating the wells. Roth and Thompson (2009) showed the value of crossplotting maximum curvature and incoherence attributes in order to delineate and map the extents of these water bearing collapse chimneys. Figure 2 shows a wellbore effectively placed between the collapse chimneys along with the micro-seismic events due to hydraulic fracturing.

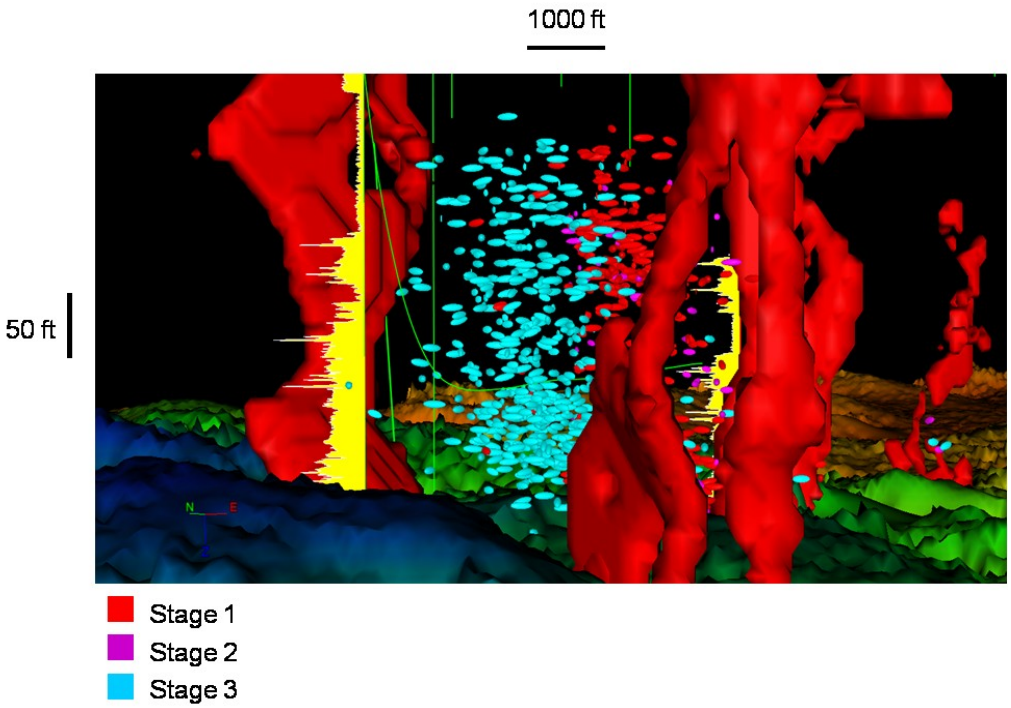

Figure 2. Volume interpretation of collapse chimneys in red displayed with interpreted seismic horizons, micro-seismic events color-coded by stage number, log type curves and wellbores. This type of modeling can help guide horizontal well placement to avoid water-bearing collapse features. (After Roth and Thompson, 2009).

Significant progress has been made in mapping natural fractures. Hunt et al. (2010) mapped natural fractures in the Nordegg chert/carbonate formation by using image logs and micro-seismic events. In order to effectively compare the fine scale image logs from the two horizontal wells to surface seismic data, they averaged the open conductive fractures from the image logs over the area of a seismic bin. These pseudo vertical wells at the 'bin' center were then compared to attributes. Multi-linear regression showed that the most useful attributes in predicting fractures was the AVAz, curvature and VVAz.

Singh et al. (2008) used discontinuity attributes to detect swarms of fractures in Kuwait from surface seismic. Their workflow uses attributes such as

coherence, Sobel-filter similarity, and curvature to delineate potential fractures. These lineaments are then processed using an ant-tracking algorithm to generate azimuthally-limited lineament (hypothesized fracture) subsets. By azimuthally-limiting the ant-tracking, they were able to generate images of lineaments (hypothesized fracture swarms) that would otherwise be masked by the dominant lineaments associated with major faulting and sealed fractures. After the fracture-sensitive lineaments were generated and processed, cores, image logs, and sonic logs and VSP's were used to predict which azimuthally-limited lineament subset corresponded to open fractures, resulting in a successful drilling program.

Narhari et al. (2009) built on the previous work by his colleagues Singh et al. (2008) and mapped large and small scale faults using seismic attributes such as coherence, edge detection, dip magnitude, dip azimuth and curvature. Image logs and cores were then used to find the dominant strike of the fracture orientations and characterize faults as open or closed. The strike of the open fractures from the image logs were found to be orthogonal to the strike of the fractures located on the seismic data. Three successful wells were drilled that showed a consistent natural fracture pattern on the image logs.

Simon (2005) showed a qualitative correlation between EUR and the extent and isotropy of the fracture network measured by micro-seismic experiments. In turn this fracture network was directly linked to P-wave anisotropic zones and parallel fractures. Higher EUR was correlated to relatively isotropic zones, resulting in a relatively orthogonal fracture pattern mapped by

microseismic events “draining” a relatively larger area. In contrast, lower EUR was correlated to more anisotropic zones with microseismically-mapped fractures “draining” a smaller area and trending parallel to the axis of maximum P-wave interval velocity.

Roende et al. (2007) applied AVAz analysis to six azimuthally sectored volumes acquired in a different area of the Fort Worth Basin. Sparse image log data confirmed the direction of natural fractures, which were then extrapolated using lateral variations in seismic anisotropy.

Refunjol et al. (2010) correlated micro-seismic event locations to 3D seismic curvature and volumetric impedance properties in the Barnett Shale. This work quantitatively showed that micro-seismic events monitored during hydraulic stimulation were correlated to both curvature features and specific ranges of P and S Impedance.

In related work, Zhang et al. (2010) shows a close spatial relationship between azimuthal anisotropy and curvature. This relationship also coincides with impedance inversion run on the azimuthally binned data.

Although seismic data and its derivative products (attributes, velocity anisotropy, AVAz) have been used to map natural fractures, to my knowledge, no one has used them to map induced fractures. Scientifically, I hope to demonstrate this capability and develop a workflow that will use 3D seismic data to extrapolate engineering data (EUR, fracability) from sparse well control to the dense seismic grid.

Devon Energy has a large inventory of 3D P-wave seismic surveys throughout the Fort Worth Basin. Originally these surveys were acquired to identify major faults in the basin so they could be avoided when drilling and completing wells. As the play has evolved into full-scale production mode, the main concern is no longer drilling into water-bearing faults because they have already been identified and mapped. Now the main concern is affecting offset wells with the completion of new wells, which could negatively impact production rates throughout the basin. Many different methods have been tried to map and predict the damaged rock from hydraulic fracturing with no positive results.

None of the surveys Devon owns are traditional time-lapse experiments. Nevertheless, for this study there are several time-lapse components. First, all the wells were logged before fracturing. Second, I know which wells produced well and which produced poorly. Third, I will have attempted to seismically map any potential damage due to induced fractures. Using these data, I anticipate to correlate sweet spots to attributes insensitive to fracture damage (time-thickness and curvature), and to map bypassed pay in areas that were thought to have been properly produced.

As part of this workflow, I will use the rich collection of image logs and micro-seismic experiments to establish a relationship between engineering practices and production data to 3D surface seismic measurements, thereby extending my workflow to areas where these ‘specialty logs’ have not been acquired. A posteriori analysis of the alternative completion designs employed during the past ten years in the survey area could provide insight into which

designs could maximize the production of new wells and prevent bashing of existing wells.

I begin with a review of the geology and production of the Fort Worth Basin. Next I evaluate the correlation of alternative attributes with EUR. Then I correlate attributes to direct fracture measurements made by image logs and micro-seismic measurements. I end with conclusions and limitations of the methodology.

CHAPTER 2

GEOLOGIC AND PRODUCTION BACKGROUND

The Ft. Worth Basin is located in north-central Texas and is a foreland basin associated with the late Paleozoic Ouachita orogeny. The basin is bounded by the Muenster Arch to the northeast, the Ouachita Thrust Front to the east, the Bend Arch to the west, the Red River Arch to the north, and the Llano Uplift to the south. Figure 3 is a map of Texas showing the extents of the Fort Worth Basin and the bounding features of the play.

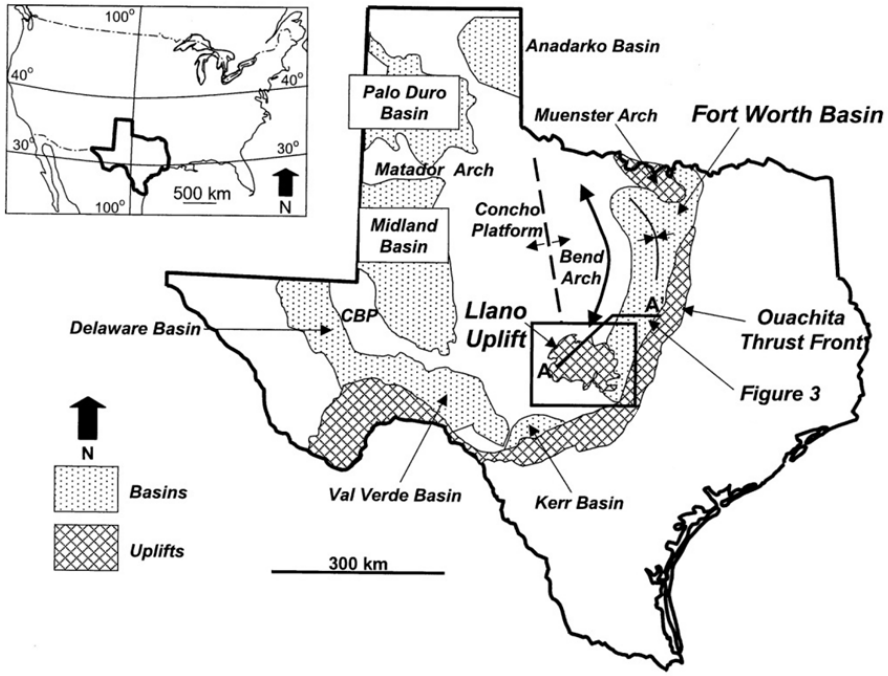

Figure 3. Map of Texas highlighting the major basins and uplifts. The Fort Worth Basin is bounded by the Muenster Arch, Ouachita Thrust Front, Llano Uplift and the Bend Arch (After Erlich and Coleman, 2005).

Deformation in the area is associated with the Ouachita orogeny and the collision of the North American craton and Gondwana (Elrich and Coleman, 1993). The target investigated in this work is the Mississippian-age Barnett

Shale (Figures 4 and 5). In the northeast portion of the basin, near the Muenster arch, the Barnett Shale is more than 90 m thick and is separated into Upper and Lower Barnett Shale sections by the Forestburg Limestone (Pollastro et al., 2007) (Figure 4). The Forestburg Limestone pinches out to the southwest of my study area, perhaps changing facies from limestone to mudstone. In this direction the Upper Barnett Shale section disappears, and the Lower Barnett thins. The Barnett sits on an angular unconformity above the Cambrian to upper-Ordovician-age carbonates of the Ellenberger Group and Viola Formation, which are characterized by collapse features. In my study area the Upper Barnett is capped by the overlying Pennsylvanian-age Marble Falls Limestone.

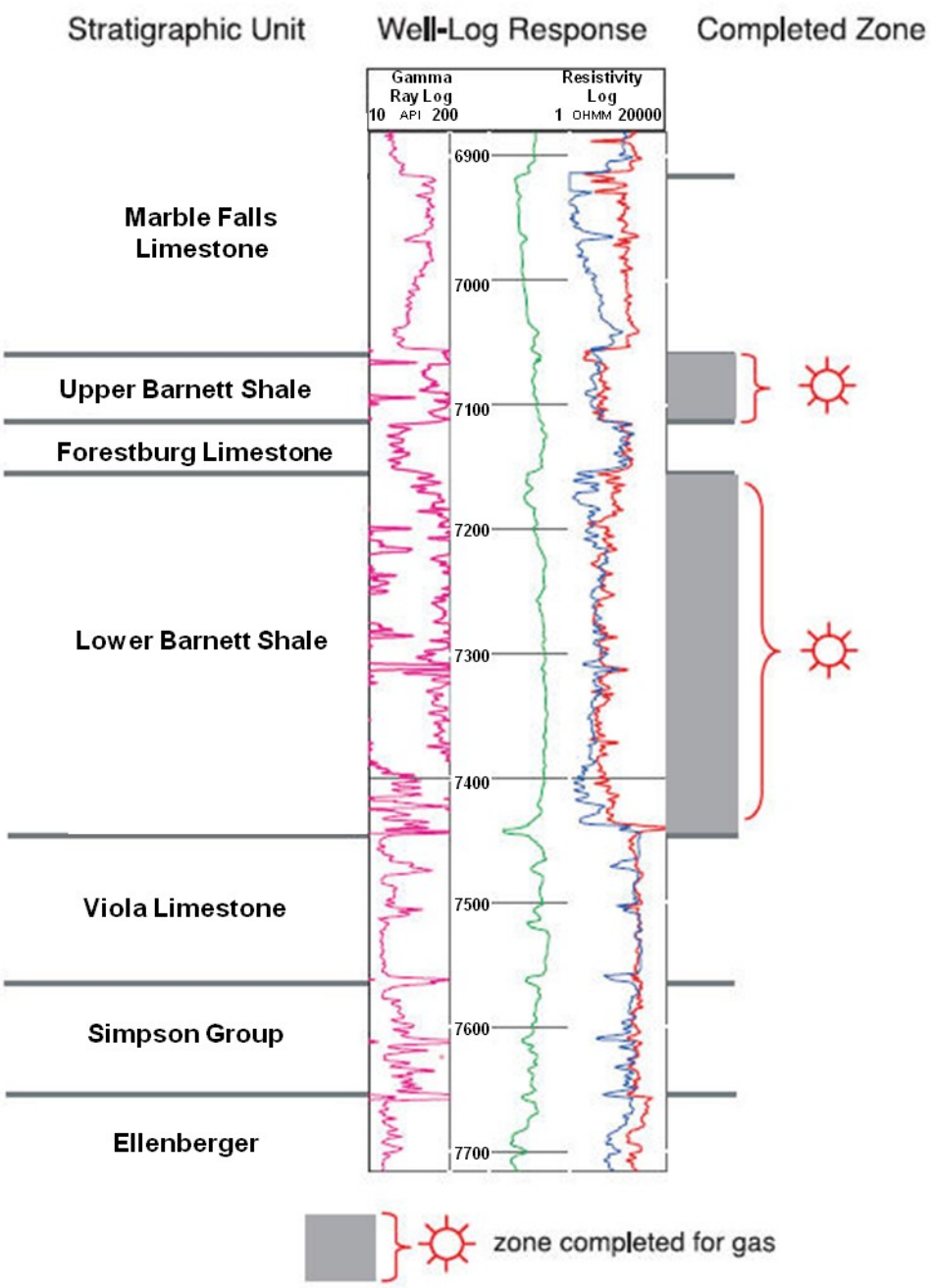

Figure 4. Simple stratigraphic section including Gamma-ray and Resistivity log responses similar to what is seen in the study area. The Deep Resistivity curve is plotted in red, while the Medium Resistivity curve is plotted in blue. The overlying Marble Falls Limestone and underlying Viola Limestone serve as frac barriers. (After Pollastro et al, 2007).

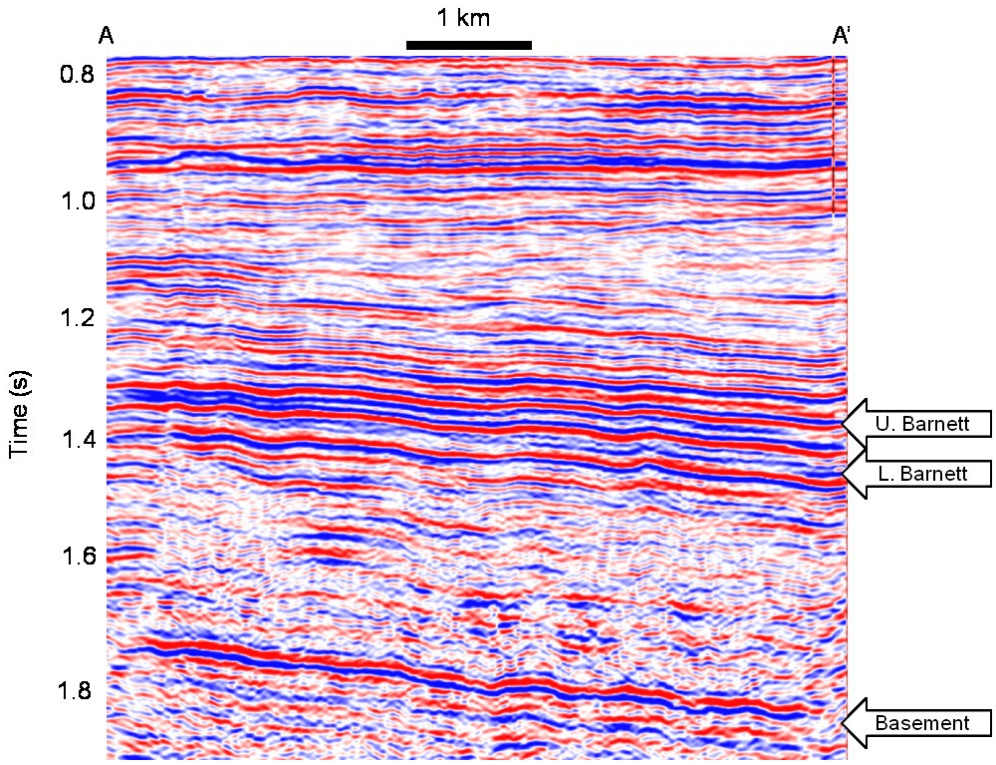

Figure 5. A west to east seismic line AA' (location shown on Figure A-1) through the 3D seismic amplitude volume indicating the location of the upper and lower Barnett horizon tops. Note the deepening to the northeast towards the Muenster Arch. (Data courtesy of Devon Energy).

The Barnett Shale is not homogeneous, but rather can be subdivided into siliceous shale, argillaceous shale, calcareous shale, and limestone layers, with minor amounts of dolomite (Perez, 2009). Portions are silica rich (up to 60%), and contain variable amounts of clay (up to 30%). It also has a high organic content, about 4-5 wt.%. Most of the Barnett Shale is thermally mature, falling within the natural gas window.

Traditionally, the Fort Worth Basin Barnett Shale gas play has been an engineering-driven play. Since the Barnett Shale dips less than two degrees and extends for hundreds of kilometers in any direction, accurate infill drilling can be achieved based on previous well top information. As an example, the 51 km^2

target area of my study area has had over 100 wells drilled without the benefit of seismic data. Ninety percent of these wells were economically successful. The relatively recent adoption of more efficient and more expensive horizontal wells has justified the use of further geologic and geophysical data.

Mitchell Energy held most of the Barnett acreage by producing from the shallower Pennsylvanian-age Atoka Sandstone. From 1982-1998, the wells in the Barnett were vertical and were completed by massive hydraulic fracture in the lower Barnett interval using CO_2 and N_2 foam or gel. In 1999, the vertical wells were 'refraced' in the lower and upper zone using slick water. The play evolved to full scale development with the introduction of horizontal well technology.

A majority of the vertical wells in the study area have been cemented and then perforated. The original completion consisted of a stage over the Lower Barnett Shale. The vertical wells that have been refraced were completed in two stages. First the lower zone of interest is perforated and hydraulically stimulated. Next a bridge plug is set above the stimulated area sealing the Lower Barnett. The Upper Barnett Shale is then perforated and stimulated. Treatment pressures are recorded for every well and plotted as a pump curve (Figure 6). Modern horizontal wells are completed in a similar fashion. In my study area the horizontal run of the wells range from 4000 ft to 7000 ft (1200 m to 2100 m), they are cemented, perforated, and commonly completed in four stages.

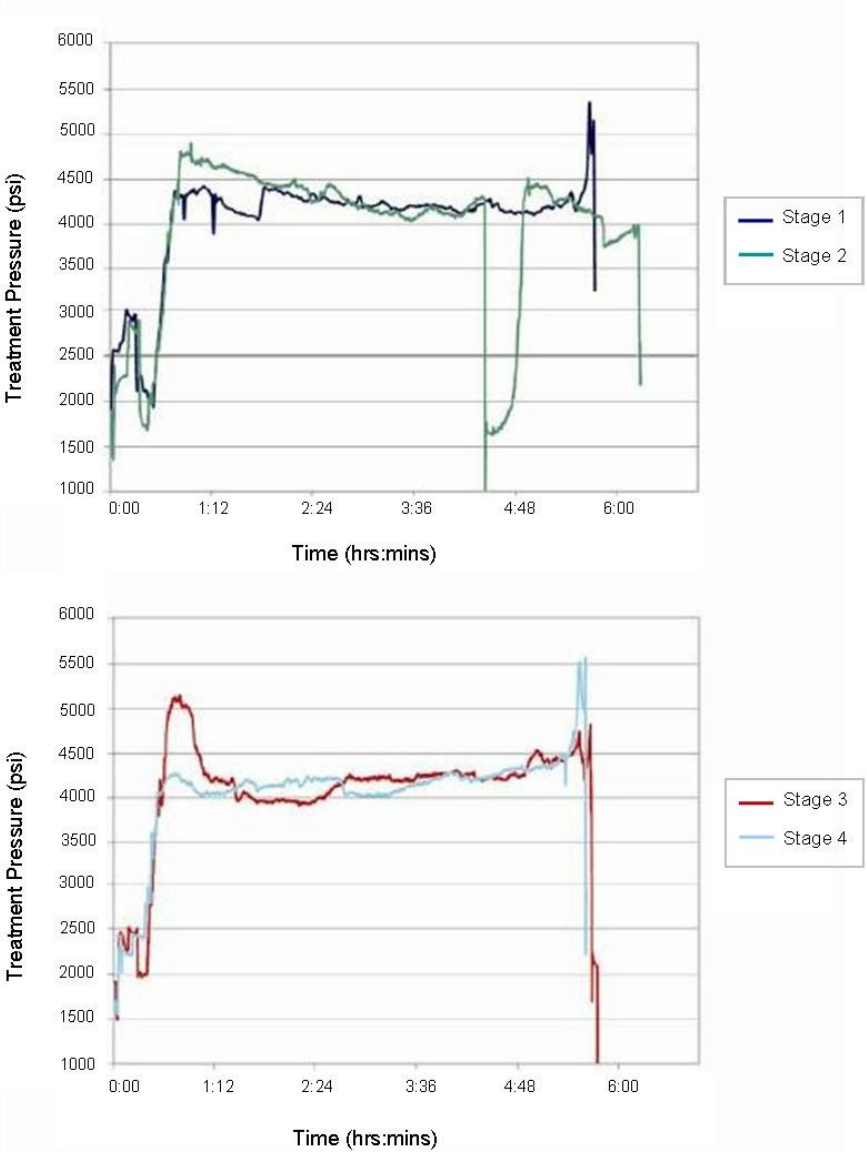

Figure 6. Sample pump curve showing treatment pressures plotted along the y axis with time along the x axis. (Data courtesy of Devon Energy).

Devon Energy acquired Mitchell Energy in 2002 and has further pushed the drilling and completion technology to improve production within the Barnett Shale. Currently 3D seismic technology is routinely used to plan, drill and design completion strategies for horizontal wells. The ideal way to interpret hydraulically-induced fractures would be to run micro-seismic, image logs, and

production logs on every well. Unfortunately, the cost of running specialty logs and micro-seismic can be equivalent to the cost of completing a well. With well densities approaching two vertical well/km^2, or one horizontal well/2 km^2, the incremental cost of a wide-azimuth high-fold 3D seismic survey is about the same cost as two vertical wells or 100% of the cost of one horizontal well. These well densities also increase the likelihood of existing wells being bashed. When a new well is hydraulically fractured and its fractured interval interferes negatively with a previously drilled well's fractured interval it is called 'bashing'. Bashing can cause the existing well (bashee) to produce water which can negatively impact its ultimate gas recovery. The basher is typically unaffected. Therefore, the ability to map damaged rock and predict the fracability of the rock from surface seismic has many positive economic implications.

When an offset well is bashed, there are three possible scenarios. The first scenario is the mostly likely case and occurs when the bashee's production is negatively affected long term. When the well is bashed it begins producing frac water and the amount of gas produced drops for a period of time. Normally, after a few days or weeks the well will regain production but it will never regain enough to follow its expected ultimate recovery curve (Figure 7a). Only rarely in this area does the bashing open conduits to the Ellenberger and lead to further water production. Such Ellenberger water production is indicated by differences in chemical composition.

The second type of bashing does not change the performance of the well long term. It is similar to the first scenario in that the well begins producing frac

water and the amount of gas drops briefly. However, this type of bashing seems to have no effect long term because production soon returns to its expected recovery curve (Figure 7b).

The third and final type of bashing is positive and increases the overall performance of the well, similar to the well being refractured. Like the previous two cases, its water production is briefly increased but it quickly drops off and the well begins tracking on a new decline curve that is higher than its original overall recovery (Figure 7c). This is the type of behavior we expect from a well that is selected for refracturing.

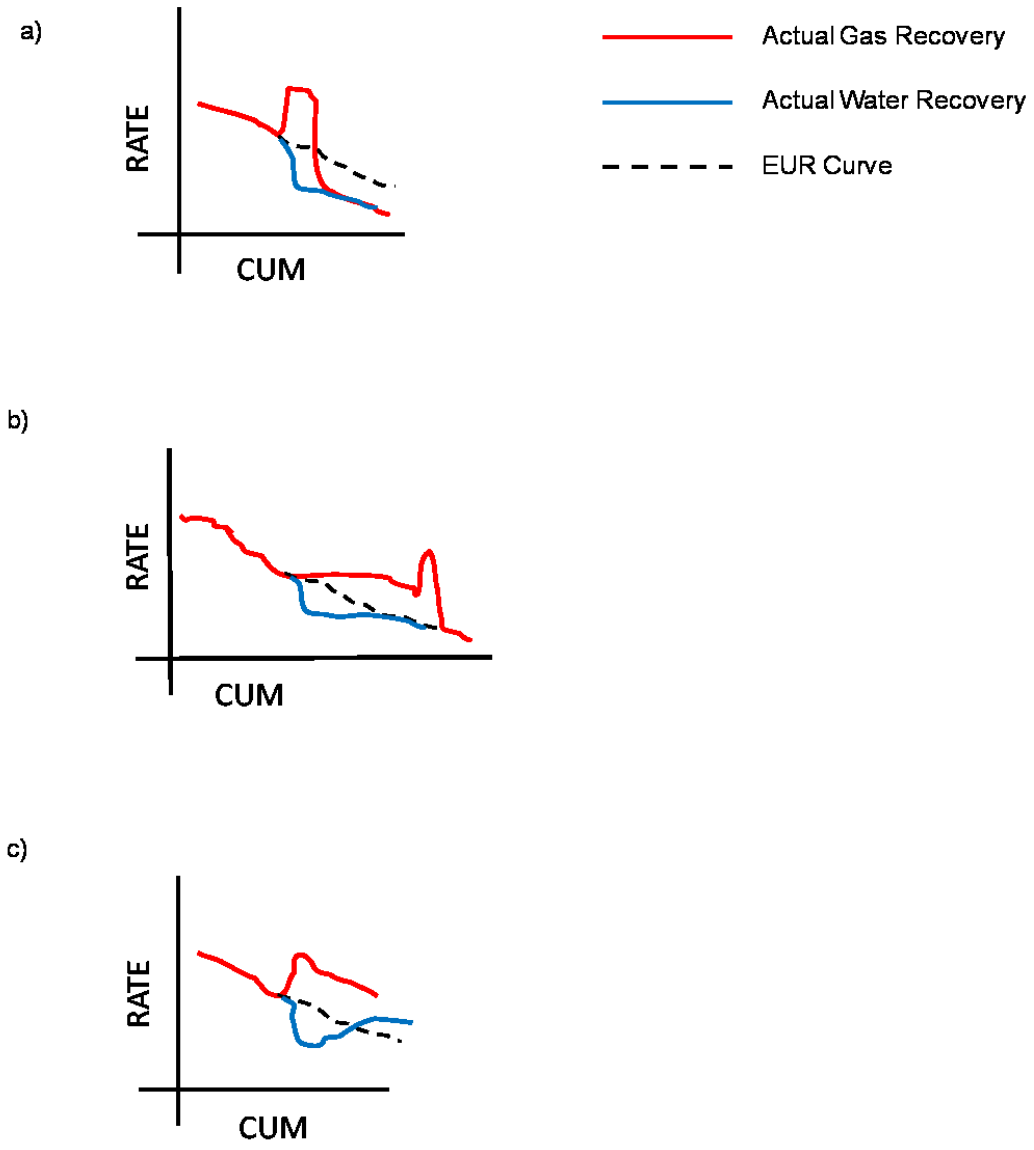

Figure 7. Example of well's production being (a) negatively, (b) unaffected long term, and (c) positively affected by bashing.

The typical candidate for refracturing is a well that has been producing for several years and has low to no production, was completed with a different type of treatment fluid to stimulate the well and/or to restore a well's production to hold a lease. Refracturing wells has proved to be very successful in increasing

ultimate recovered production by either re-opening existing induced fractures or creating new induced fractures within the reservoir.

The majority of existing wells in the study area are vertical. It is critical to better understand the behavior of bashed and refractured wells to properly design future well locations and improve well completions. With improved well placement and well completions to avoid existing fractured areas and target un-fractured areas ultimate recovery will improve. One way to better understand fracture behavior is through the use of high quality 3D P-wave seismic surveys. These data sets are more consistent in acquisition practices and are present over a majority of Devon acreage. Unlike production or geologic log data, seismic data can provide lateral information away from the wellbore.

A new 3D seismic program was completed in 2009, and horizontal wells are now being in-filled between the existing vertical wells to produce by-passed pay. Successful mapping of the zones of hydraulically fractured rock and correlation of the volume of the fracture zone with production will have a large impact on cost and ultimate gas recovery. In addition, this study provides a means of a posteriori validation of alternative fracture and well placement strategies used during the past that can be used to improve development efficiency in this and other areas of the Fort Worth Basin and possibly in other basins.

CHAPTER 3

CORRELATION OF INDUCED FRACTURES TO SEISMIC MEASUREMENTS

Devon's Barnett wells in this survey are considered to be producing from open, gas-filled fractures. If I assume orthorhombic symmetry corresponding to horizontal lamination and one dominant set of vertically-aligned open fractures, I hypothesize that I should be able to detect open fractures with surface P-wave seismic (Lynn 2004). Orthorhombic symmetry is one set of vertically aligned fractures; or two vertical sets that are orthogonal; plus the layer anisotropy. Vertical wells that have been refraced do not fit this hypothesis so they are left out of the study. Wells that have been refraced are believed to have more than one set of fractures due to evidence from micro-seismic experiments and increased production rates after refracturing. I also expect the seismic signature detected at well locations to vary by azimuth due to the hydraulically induced fractures. Knowledge of fast- and slow-velocity azimuthal directions in this survey, from previous seismic experiments, as well as the behavior of the micro-seismic data will aid in confirming this expectation.

Most-positive curvature and velocity anisotropy are known to be good predictors of fracture orientations (Figure 8). If there are pre-existing structural features (faults, flexures, etc.) that occurred in the geologic past, we anticipate the the P-wave anisotropy to be influenced by these pre-existing zones of weakness. In my area, these pre-existing structures are either a single set of vertical aligned fractures or multiple sets of vertical fractures. For simplicity, I assume that if there are more than one fracture set, only one will be parallel to

the maximum horizontal stress and open at the present time. The fast direction of the P interval velocity is interpreted as parallel to the open fracture network and the maximum horizontal stress (Lynn, 2010). When interval velocity fast minus slow is large and interval velocity maximum is high this is indicative of one set of cracks; but when interval velocity fast minus slow is large and interval velocity is low it is indicative of two sets of orthogonal cracks. Multiple sets of vertical cracks appear as random azimuths, low interval velocity fast-slow, and low maximum interval velocity.

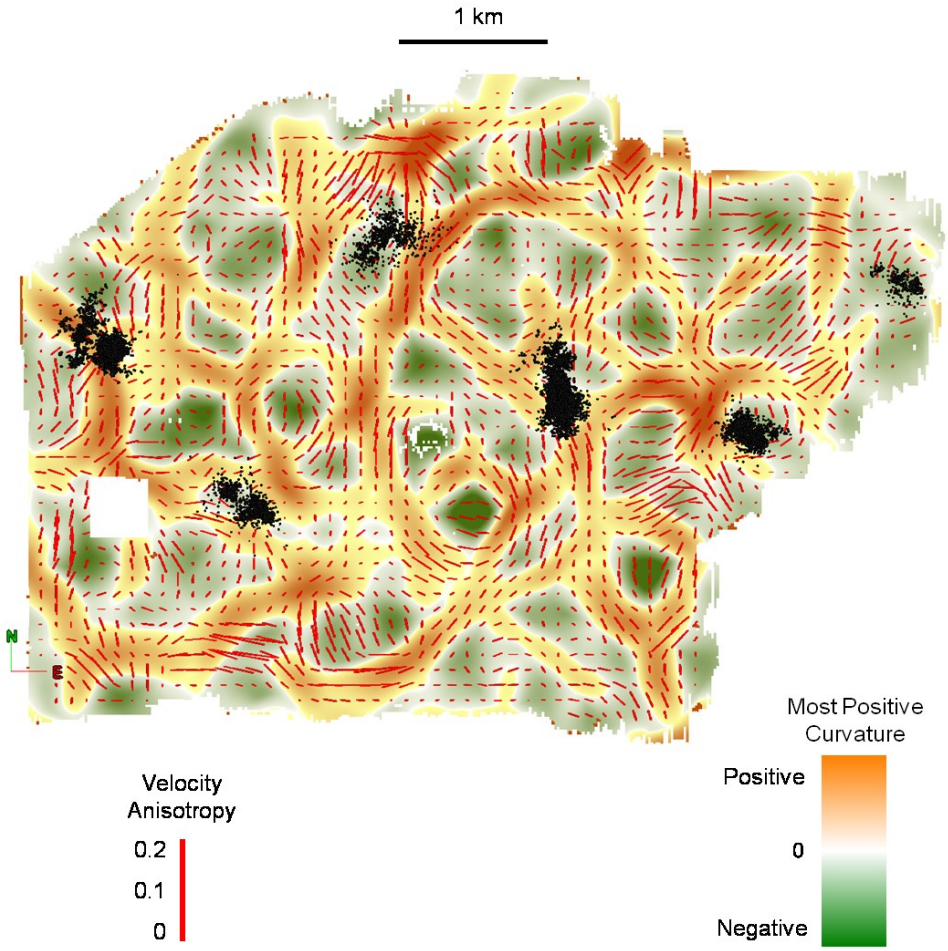

Figure 8. Velocity anisotropy (red vectors) displayed with most positive curvature extracted along the top of the Viola limestone. The length of the vector is proportional to the degree of anisotropy while the direction indicates the azimuth of maximum anisotropy. Micro-seismic events are shown in black . Even though all horizontal wells were drilled NW-SE and the regional maximum horizontal stress in NE-SW, note how the micro-seismic events and the velocity anisotropy trend in multiple azimuthal directions. Note also the clustering of microseismic events in structurally low areas, suggesting that the ridges may serve as fracture barriers.

Typically seismic attributes are run on full-azimuth, full-offset stacked data. In our study a full suite of 180 attributes were run by a third party vendor on each of the four azimuthally-sectored PSTM volumes. A total of six horizons, located both above and below the zone of interest were picked on each azimuthally-

sectored volume to avoid the overprint of the expected velocity anisotropy that would otherwise result in azimuthally-variable time-delays.

For this analysis, three horizons above the zone of interest were chosen, plus one at the top of the Barnett Shale, one within the Barnett Shale and one below. Two of the six horizons were not picked on a reflector, but were phantom horizons 20 ms above the picks to validate the azimuthal variations that were being seen on a horizon and ensure that we were not missing any attributes that may be varying within the zone of interest. Analyzing anisotropy along multiple horizons provides a means of differentiating azimuthal variability in the hydraulically-fractured target, and 'natural' anisotropy expressed in the underlying and overlying fracture barriers. The attribute values, extracted at each horizon for the 180 attributes of each of the 4 azimuth sectors (4320 horizons), are then fit to an ellipse using a workflow designed by Gretchka and Tsvankin (1998) to analyze NMO velocity in a medium with horizontal transverse symmetry. Following the methodology of Thompson et al. (2010) ellipses were fit for each attribute (see Appendix B). After the ellipse fitting on the individual horizons, we ranked the attributes by the highest reliability, R, given by equation B7, for each horizon. The reliability is not intended to measure the goodness of fit, but rather how well determined the azimuthal measurement is for a given attribute. The reliability is inversely proportionate to the RMSE and proportionate to eccentricity. As the RMSE decreases or as the eccentricity increases the azimuth of the angle is well-determined and therefore reliable. As λ_1 approaches

λ_2, the azimuth becomes poorly determined making it less reliable for ellipse fitting.

I also computed the best-fit ellipse on a set of random data in order to test the statistical significance. The median reliability for a random data set was 5.1. Median reliabilities calculated on the horizons ranged from about 4 to 7. Attributes with reliability near 4 were inappropriate for ellipse fitting and were discarded. A value of R greater than 6 is considered a statistically significant fit.

A list of the top 10 attributes with the highest reliabilities was made for each of the 6 horizons. From the individual lists we selected 25 attributes for a more in-depth review (Table 1). The 25 selected attributes consisted of several attributes that appeared in the list of multiple horizons' top reliabilities and some attributes that only appeared in one horizons' top reliability list. Among the highest ranked attributes were several of the spectral decomposition components. I computed Gabor-Morlet decomposition amplitude, magnitude, and phase estimates ranging from 10 Hz to 90 Hz at 5 Hz increments. Kalkomey (1997) warns of false correlations when using too many attributes to predict geologic features of interest. When there is insufficient control to statistically validate attributes, she suggests that only attributes with a physical (rather than simply statistical) reason to be correlated with a feature of interest should be used. While many other attributes show good reliability, the lower frequency spectral decomposition components have well-established sensitivity to thin bed tuning (e.g. Widess, 1973), and therefore to azimuthal variation in velocity which correlates to my best reliabilities occurring in the frequency range from 10-35 Hz.

Next, the eccentricity, *e*, given by equation B6 was mapped and compared for the top 25 attributes for each horizon. Eccentricity maps were compared between all horizons. Mapping the 25 attributes' eccentricities showed 15 attributes with valid results. Table 1 shows the list of high reliability, valid eccentricity attributes.

Table 1: List of 25 azimuthally sectored attributes with high ellipse fit reliability

10 Hz spectral magnitude	Imaginary Component
15 Hz spectral magnitude	Real Component
20 Hz spectral magnitude	Envelope Derivative
25 Hz spectral magnitude	Acoustic Impedance
30 Hz spectral magnitude	Wavelet Attributes
35 Hz spectral magnitude	Wavelet Dominant Frequency
25 Hz spectral phase	SOF amplitude
10 Hz spectral trace	TWT (or uncorrected picks)
15 Hz spectral trace	Imaginary Trace
20 Hz spectral trace	Mean Frequency
25 Hz spectral trace	Q Frequency Shift
30 Hz spectral trace	RMS Frequency
35 Hz spectral trace	

All spectral components were computed with a Gabor-Morlet decomposition. Definitions in Appendix C

The first difference between the eccentricity maps was noticed between the Lower Barnett Shale and the Viola Limestone. Figure 9b shows the degree of eccentricity is larger at the top of Viola Limestone than at the top of the lower Barnett shale (Figure 9a) indicating a different fracturing regime within the Barnett. Figures 10a and 10b show the reliability calculated at the lower Barnett

shale and Viola Limestone. Anywhere the map is red the fit is valid, which confirms our use of this attribute.

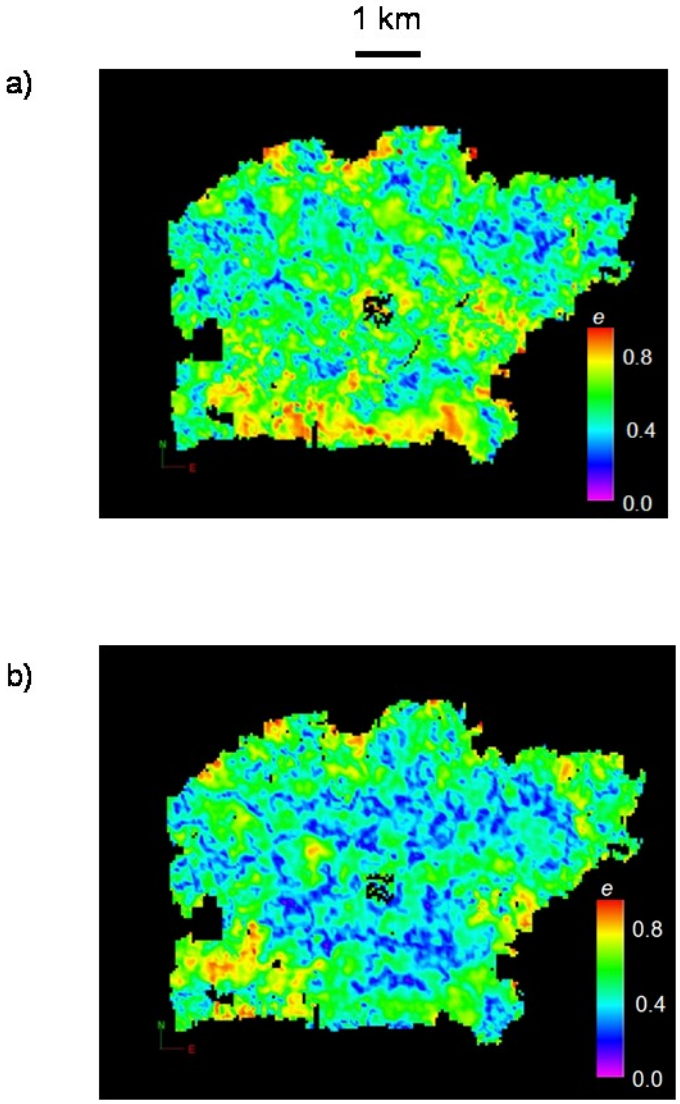

Figure 9. Example of wavelet dominant frequency amplitude azimuth eccentricity maps calculated using equation B6 on (a) the top of the Lower Barnett Shale and (b) along the top Viola.

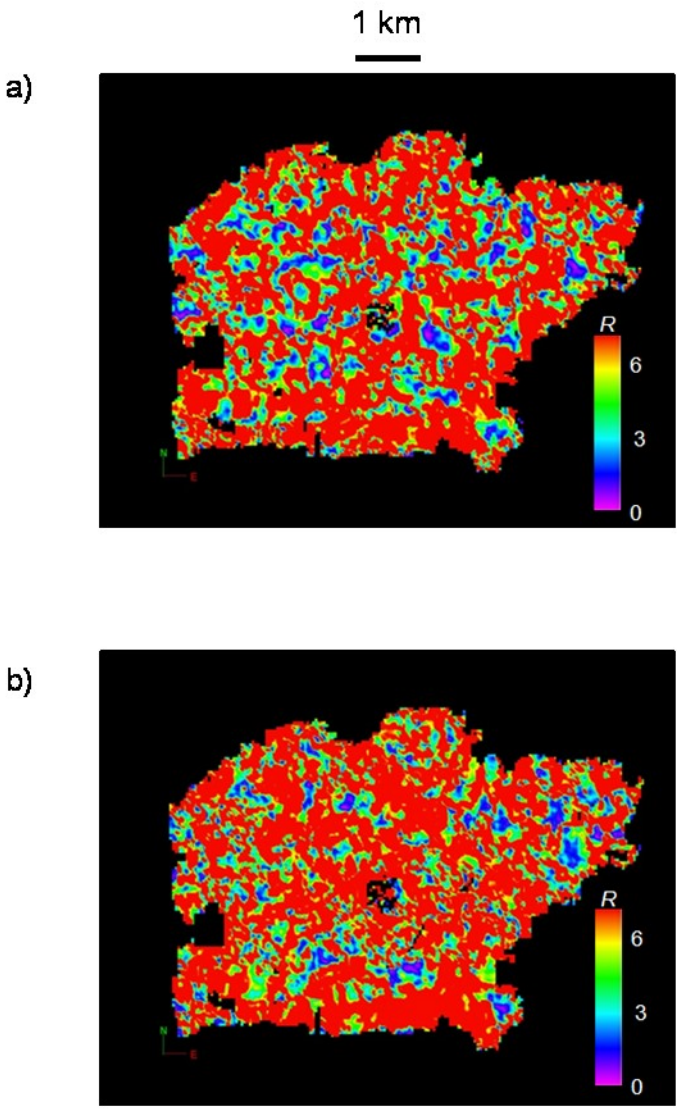

Figure 10. Example of reliability maps calculated on (a) the top of the Lower Barnett Shale and (b) the top Viola. Any area where the map is red is a statistically reliable fit and confirms the use of the attribute.

In order to further exploit differences between the horizons I investigated the correlation of eccentricities by crossplotting the Marble Falls versus the Lower Barnett Shale. This interval was chosen because the Marble Falls is a competent, un-fractured formation and the top of the Lower Barnett Shale is a highly fractured reservoir so the degrees of eccentricity are expected to be

varying more between these two intervals than between the Lower Barnett Shale and the Viola Limestone. From crossplotting, four attributes of Gabor-Morlet Spectral Components, Wavelet Envelope Derivative, and Wavelet Dominant Frequency were found to have poor correlations between the Marble Falls and the Lower Barnett Shale.

Next, I looked at the ellipse fit azimuths for the four attributes that had poor correlations between the Marble Falls and the Lower Barnett Shale. If orthorhombic symmetry is present, one dominant azimuth direction would be expected. Rose diagrams were created for the azimuths on each of the four horizons, Marble Falls, Forestburg Limestone, Lower Barnett Shale and the Viola Limestone. Figure 11 shows each attribute has an increase in azimuth directions within the Forestburg and the Lower Barnett Shale and a change in dominant azimuth direction.

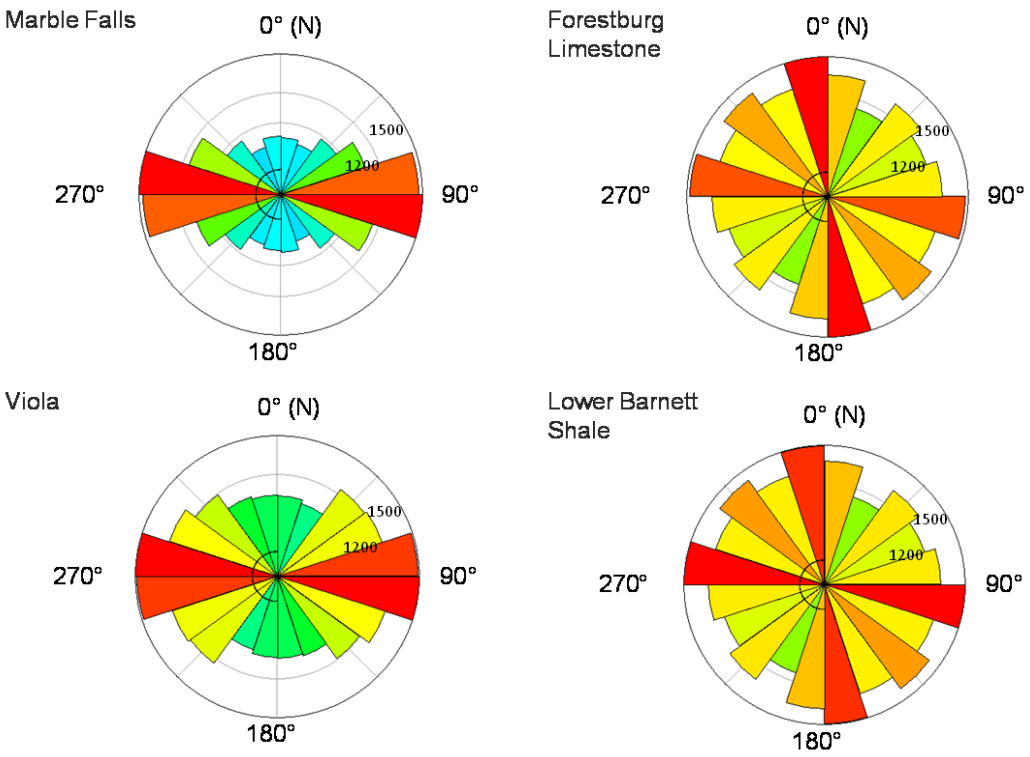

Figure 11. Rose diagrams showing the wavelet dominant frequency azimuth of the best fit ellipse for the Marble Falls, Forestburg Limestone, Lower Barnett Shale, and Viola. Note the difference between the rich variation in azimuth of the hydraulically-fractured Forestburg Limestone and Lower Barnett Shale and the strong E-W azimuth in the overlying Marble Falls and underlying Viola Limestone fracture barriers.

Finally the azimuths were compared with the eccentricities. Figure 12 displays the azimuth directions using a cyclical colorbar blended with the eccentricities in grayscale for each of the four horizons. Larger eccentricities appear black while smaller eccentricities are transparent. These maps show there are higher eccentricity values for the Marble Falls Limestone and the Viola Limestone with lower values for the Forestburg Limestone and the Lower Barnett Shale implying the competent, un-fractured Marble Falls and Viola Limestone are more anisotropic than the known fractured interval. This also disagrees with our

assumption of orthorhombic symmetry and suggests a more complex, induced fracture orientation.

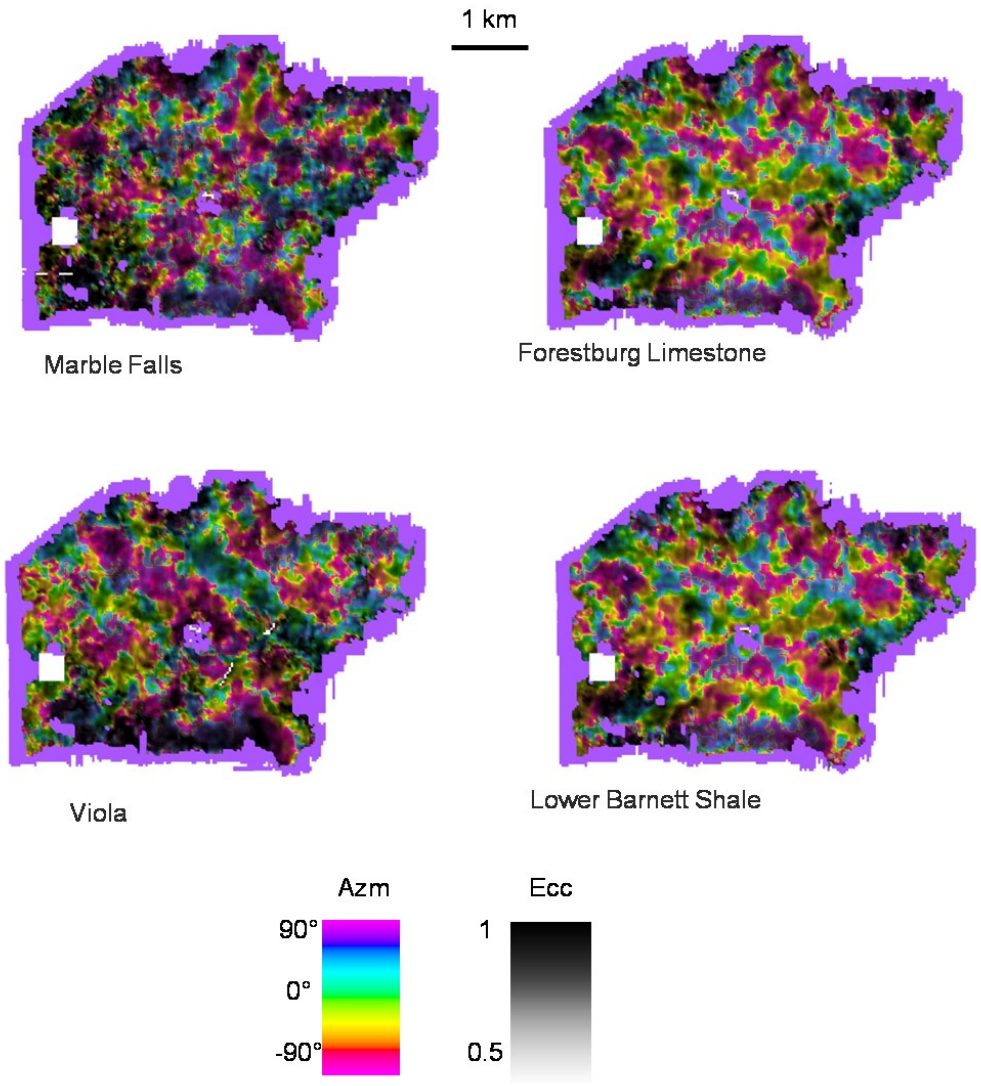

Figure 12. Maps showing the azimuth of the ellipse fit blended with the eccentricity of the Wavelet Dominant Frequency for the Marble Falls, Forestburg Limestone, Lower Barnett Shale, and Viola. Notice the greater frequency of azimuths and within the Forestburg and Lower Barnett Shale and greater eccentricities in the Marble Falls and Viola.

In the next sections I discuss comparing these attributes with production and specialty data to map the hydraulically-induced fractures and confirm the finding of more than one dominant fracture direction.

CHAPTER 4

CORRELATION OF PRODUCTION TO SEISMIC MEASUREMENTS

I begin by evaluating the wells according to their EUR. For data sensitivity reasons, actual EUR values are scaled to range between 0 and 10. These scaled EUR values will be compared to the total production up to April 2009 and January 2010. My hypothesis is that the ratio of gas produced up to April 2009 and January 2010 to EUR should provide an estimate of gas produced which should be proportional to the open fracture surface area. Wells with smaller ratios should indicate more open fractures because it would be early in the production decline curve for the well. Conversely, wells with larger ratios should indicate fewer open, conductive fractures and would have produced more of their expected ultimate recovery. Figure 13a shows a sample decline curve and Figure 13b shows where the wells are expected to plot along the curve.

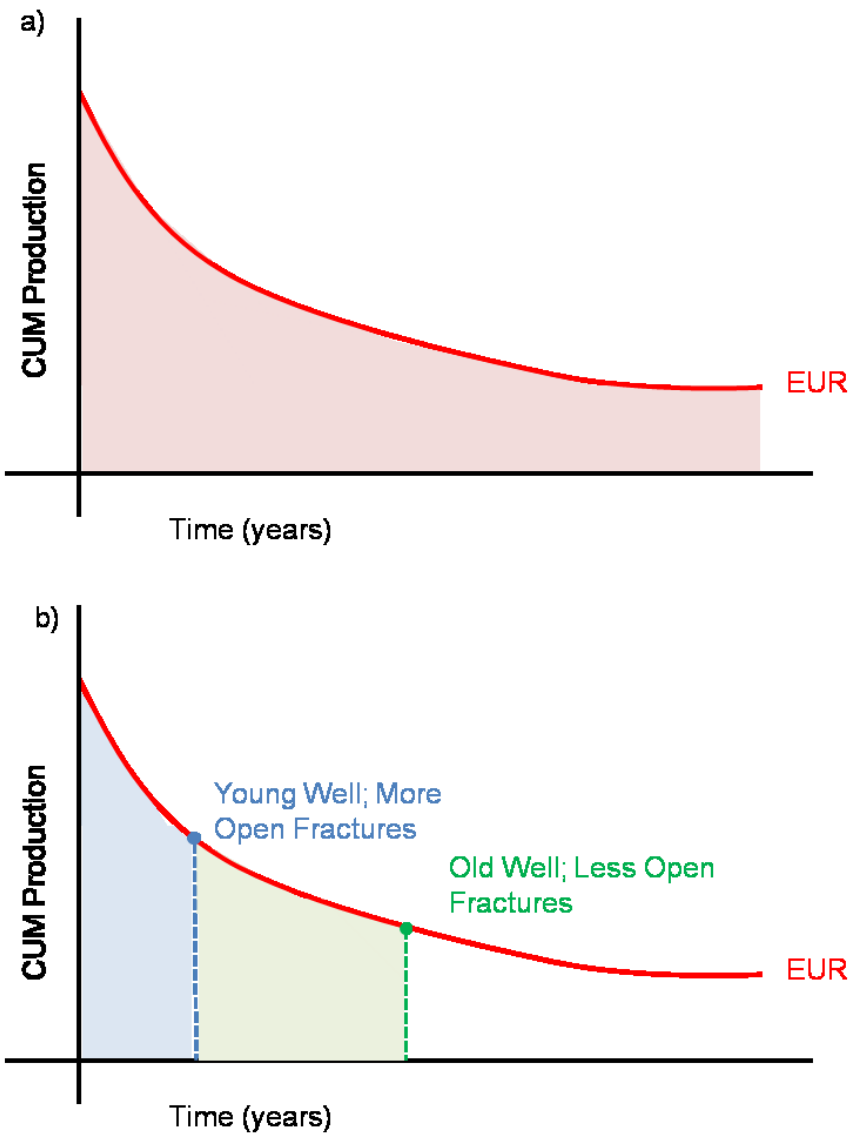

Figure 13. (a) Idealized decline curve of expected ultimate recovery (EUR). (b) Cartoon showing where wells plot along the curve during different times in their production history.

The data from vertical wells is somewhat simpler to analyze and has been filtered by wells that have not been refraced. These data are not easily gridded without smoothing because of their rapid spatial variability. Figure 14 shows the non-refraced vertical wells' April 2009 production divided by EUR gridded at 550 feet by 550 feet, while Figure 15 shows the non-refraced vertical wells' January

2010 production divided by EUR gridded at 550 feet by 550 feet. The maps of April 2009 production divided by EUR and January 2010 production divided by EUR show little differences due to the short amount of time between the time the survey was shot and the data collected. The EUR values from the horizontal wells are more challenging to post and correlate and need to be normalized by lateral length and the number of stages. Figure 16 (black inset) illustrates the problem with gridding the horizontal wells along with the non-refraced vertical wells. When the production is gridded and mapped it is assigned to the bottom-hole location for the horizontal wells. The wellbore is known to be producing from other zones throughout the lateral and away from the wellbore so the map is not adequately reflecting this. However, gridding the EUR values for all wells, horizontal and non-refraced vertical wells, shows a better correlation with the seismic products (Figure 1).

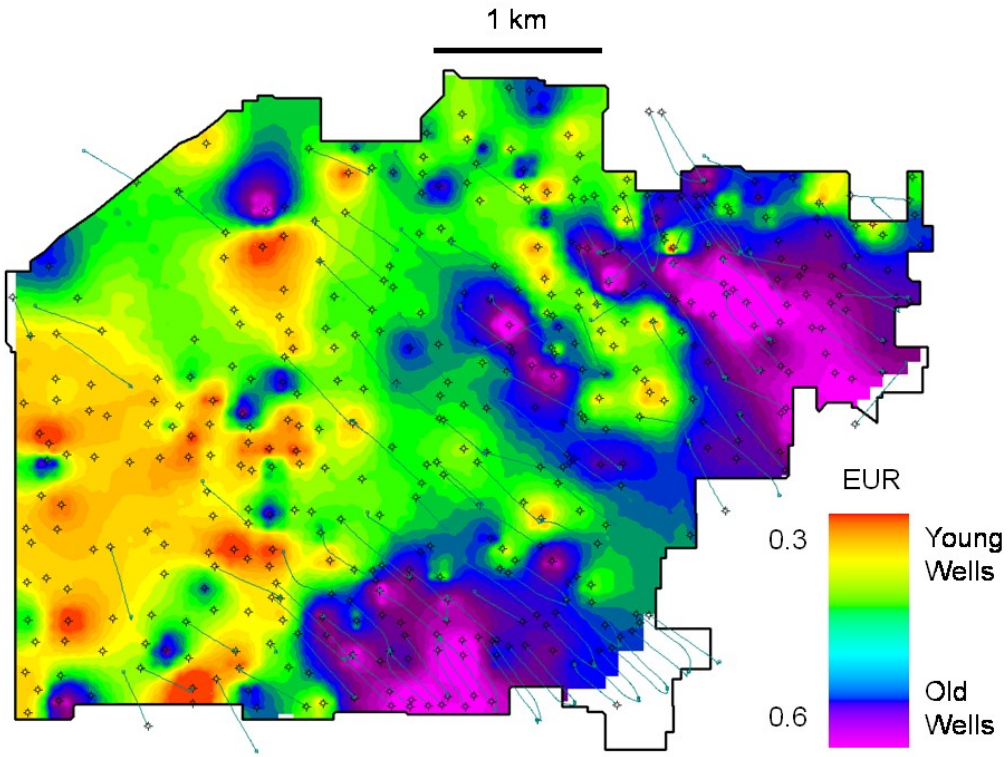

Figure 14. Relative wells' April 2009 production divided by EUR values mapped using a 550 ft by 550 ft grid. All 435 wells completed before April 2009 are mapped, but only the 175 vertical wells that have not been refraced are gridded. Red areas on the map are indicative of more induced fractures because the well has been producing a shorter amount of time and has a smaller ratio of cumulative production vs. EUR.

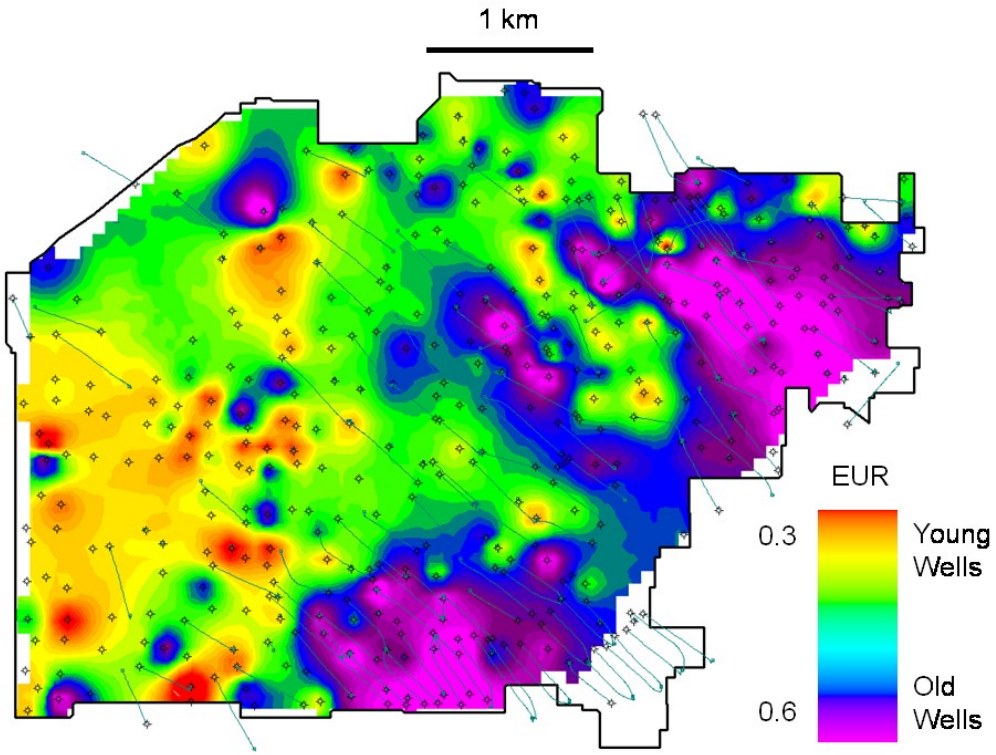

Figure 15. Relative wells' January 2010 production divided by EUR values gridded at 550 ft by 550 ft. All 435 wells completed before April 2009 are mapped, but only the 175 vertical wells that have not been refraced are gridded. Red areas on the map are indicative of more open induced fractures because the well has been producing a shorter amount of time and has a smaller ratio of cumulative production versus EUR.

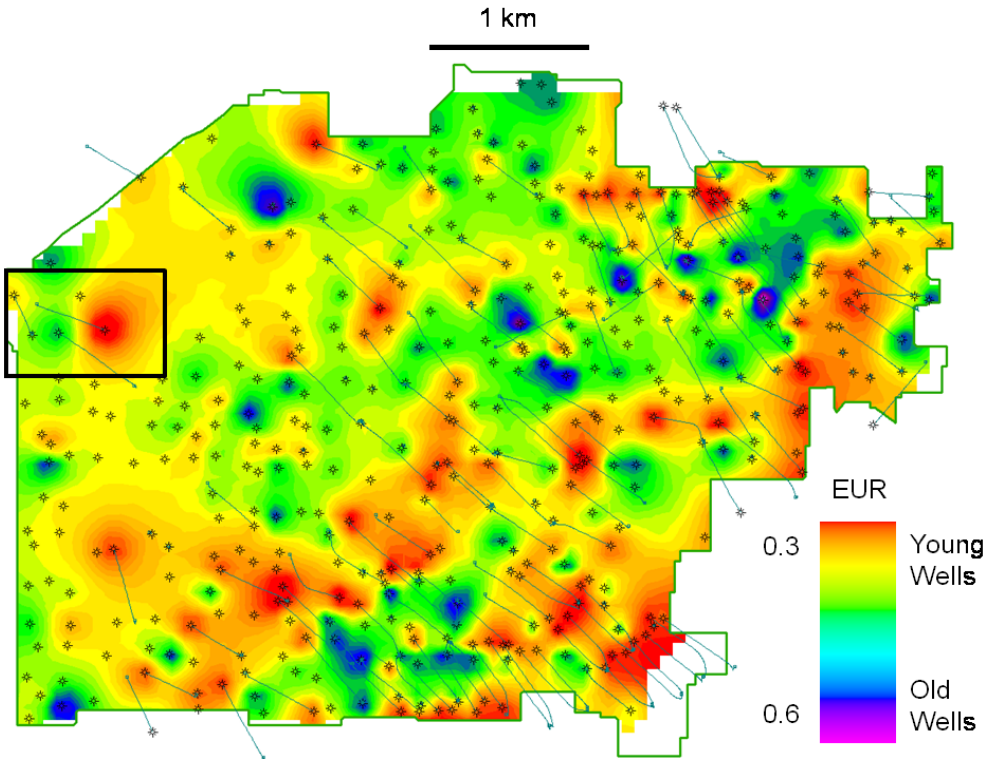

Figure 16. Relative wells' April 2009 production divided by EUR values gridded at 550 ft by 550 ft. All 435 wells completed before April 2009 are mapped, but only the 175 vertical wells and 126 horizontal wells that have not been refraced are gridded. Red areas are indicative of more open induced fractures because the well has been producing a shorter amount of time and has a smaller ratio of production versus EUR. The horizontal well with inside the black rectangle represents the issue of gridding horizontal wells. The software does not evenly distribute the value along the length of the lateral, it only places the value at the bottom hole location resulting in bulls-eyes.

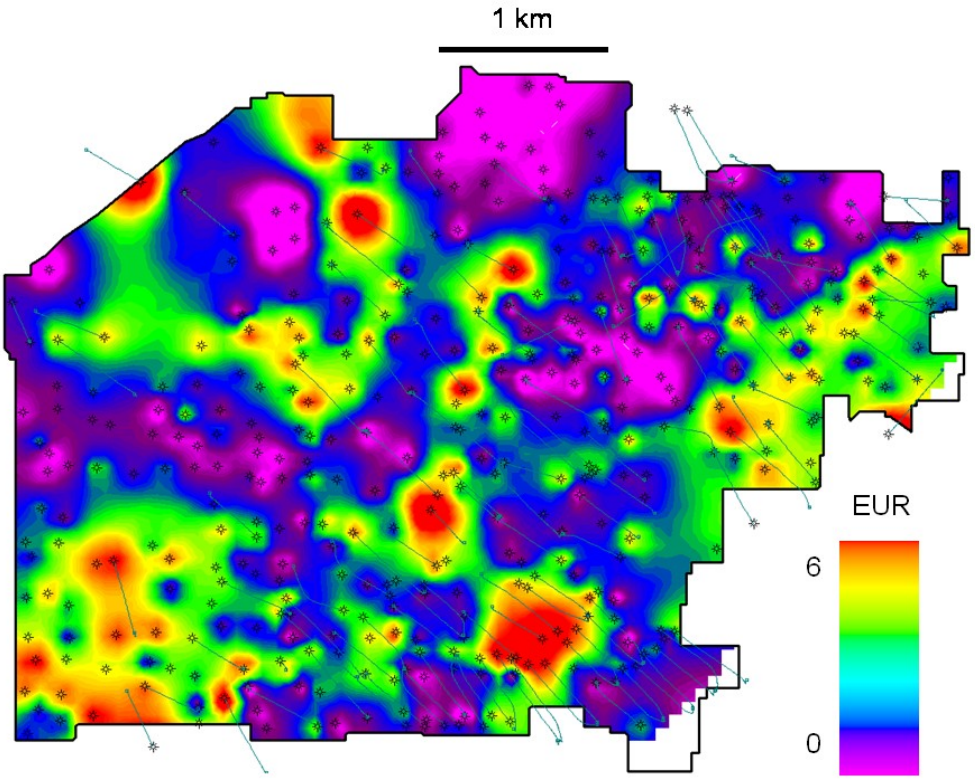

Figure 17. Relative EUR values mapped using a 550 ft by 550 ft grid using all 435 wells completed before April 2009. Red areas indicate larger EUR values corresponding to better producing wells.

A visual correlation between EUR and most-positive curvature has been seen in other surveys within the Ft. Worth Basin and can also be applied to this study survey. Statistical correlations, however, are very poor due to the wells' complex fracture histories. Figure 18 shows most-positive curvature displayed in grayscale blended with EUR values from all horizontal and vertical wells drilled and completed prior to April 2009 displayed in color. Areas of negative values of most-positive curvature are transparent and correspond to areas of higher relative EUR values shown in the yellow to red. The areas of most-positive curvature also appear to segregate the higher EUR values. Figure 19

demonstrates that the visual correlation is not as convincing when horizontal and refraced vertical wells are excluded. This EUR map of only non-refraced vertical wells is also quite similar to the April 2009 production divided by EUR map and the January 2010 production divided by EUR map. For this reason and the lack of correlation with production, only EUR values for all wells completed before April 2009 will be considered further in the study.

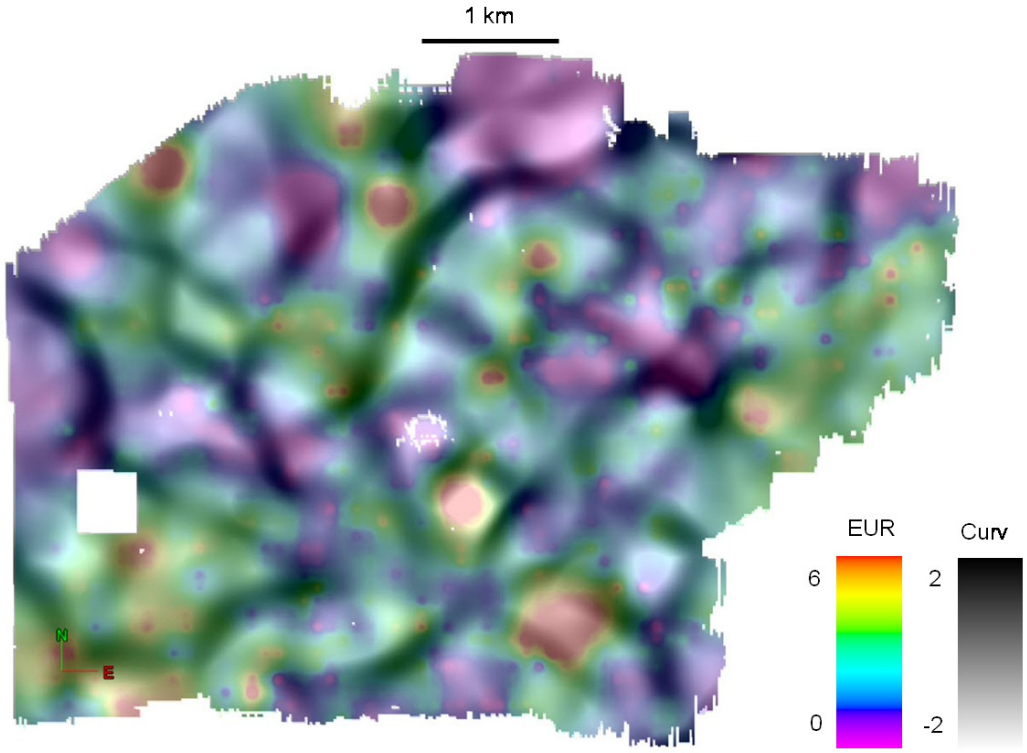

Figure 18. The EUR image displayed in Figure 20 co-rendered with most positive curvature. Most positive curvature is displayed as a grayscale with negative values being transparent and positive values being black. Notice the larger EUR values are compartmentalized by the most positive curvature ridges.

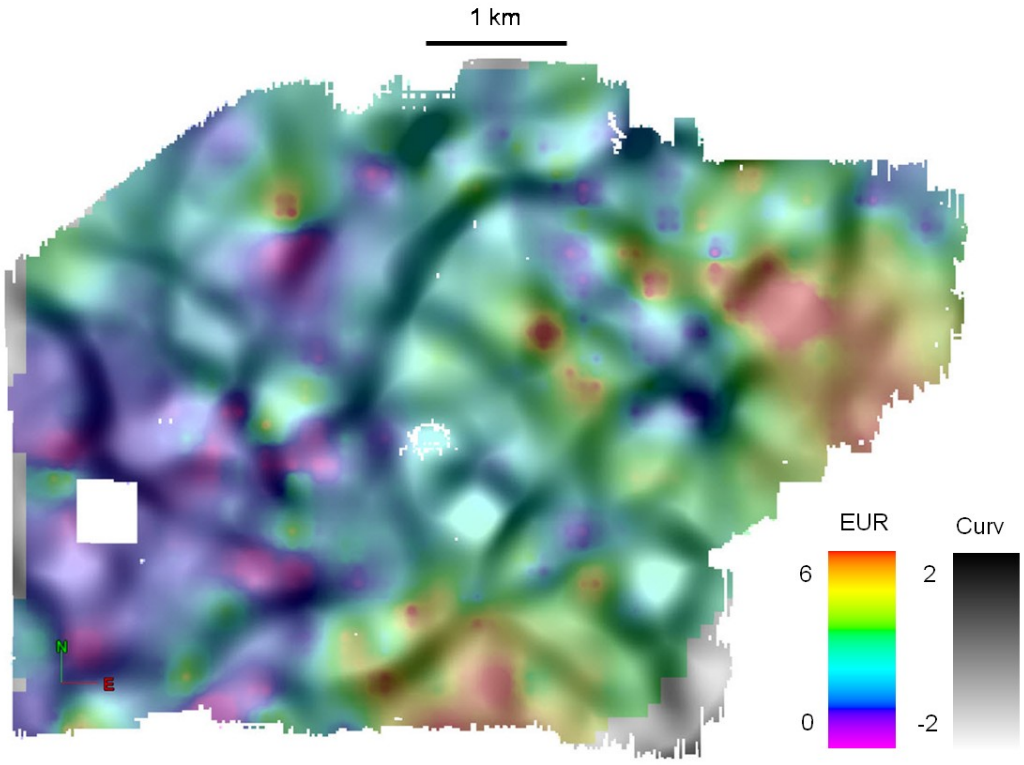

Figure 19. Relative EUR values gridded at 550 ft by 550 ft displayed with most positive curvature. All non-refraced vertical wells completed before April 2009 (175) are gridded. Where the map is red are larger EUR values which are better producing wells. Most positive curvature is displayed as a grayscale with negative values being transparent and positive values being black. Notice the correlation is not as strong when all wells are used.

Next production was compared with the ellipse fit attributes. The EUR maps were smoothed too much to be compared to the ellipse fit eccentricity values, which are very spatially variant. Instead, the known visual correlation between most-positive curvature and EUR was used to display eccentricity values of Gabor-Morlet Spectral Components with most-positive curvature. Figure 20 shows there is not a good relationship between curvature and eccentricity values. These attributes are also likely to be uncorrelated due to the complex fracture history in this area.

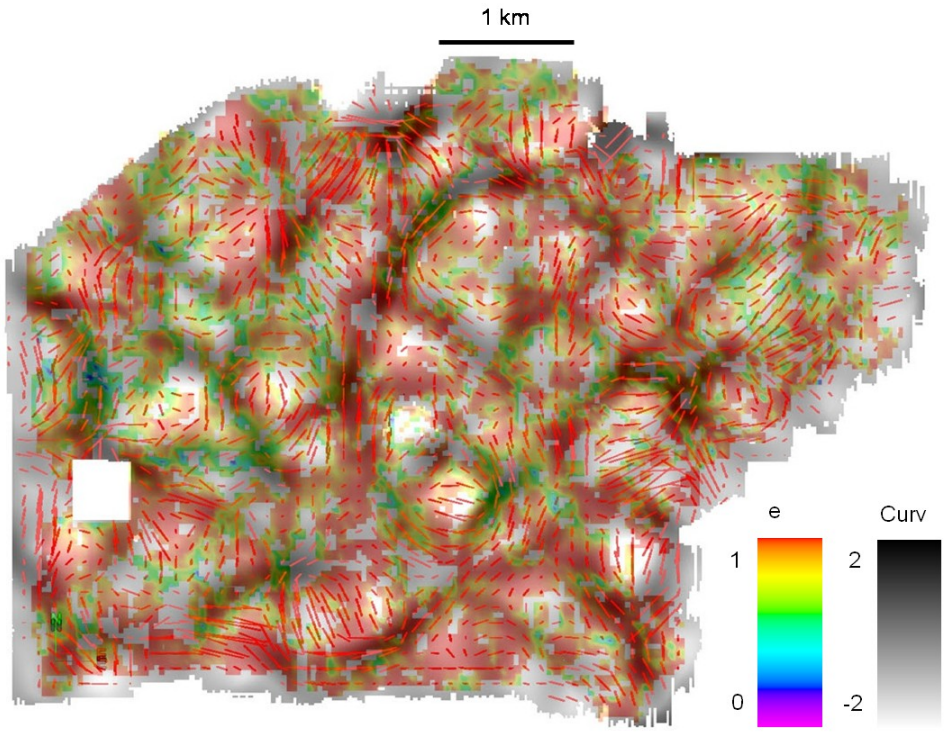

Figure 20. Eccentricity values, e, computed by applying equation B6 to the 35 Hz magnitude of the Gabor Morlet spectral component along the Lower Barnett Shale. Eccentricity is co-rendered with most positive curvature and velocity anisotropy. Red areas indicate eccentricity values. Most positive curvature is displayed as a grayscale with negative values being transparent and positive values being black. The length of the vector is proportional to the degree of anisotropy while the direction indicates the azimuth of maximum anisotropy. Notice there is no real correlation between the eccentricity and most positive curvature or velocity anisotropy.

Chapter 5

CORRELATION OF SEISMIC MEASUREMENTS TO DAMAGED ROCK

I have two means of directly measuring the azimuth and intensity of damaged rock: through the use of image logs run before the stimulation process and through micro-seismic events run after the stimulation process.

The use of image logs has increased exponentially over the last few years and has become much more commonplace in the standard suite of logging while drilling (LWD) tools used in the Barnett Shale. Information derived from these images include detection of natural and drilling induced fractures, estimation of the density and orientation of the fractures, indication of which fracture sets are open and through fractures induced by drilling before hydraulic fracturing measures of the maximum stress direction around the borehole (Quinn et al., 2008). This information is used to better place, orient, drill and complete future wells.

Fracture distribution can vary within a basin and can make the difference between average or good producing wells (Quinn et al., 2008). In the Barnett Shale the best performing wells appear to be drilled in areas that do not have any pre-existing fracture networks. The existence of pre-existing fracture networks are usually caused by stimulation from offset wells, tapping into these fracture networks will lead to the bashing of producing wells and loss of fracture energy to break new rock. To optimize the hydraulic stimulation program, it is necessary to obtain information about the type, location, frequency and direction of fractures (Janwadkar et al., 2007).

I interpret the East-West dominant azimuthal frequency in the Marble Falls Limestone to likely be East-West aligned fractures and/or local maximum horizontal stress. Although the regional maximum horizontal stress for the basin is N45E, this survey lies between two strike slip faults, and a rotation of the local stress field is interpreted. Image logs drilled before the well was hydraulically stimulated show a similar direction of stress in the Marble Falls as the envelope weighted wavelet frequency amplitude azimuth maps. Figures 21a and 21b show the azimuthal amplitude map with the well location of the image log and the image log azimuth of interpreted fractures.

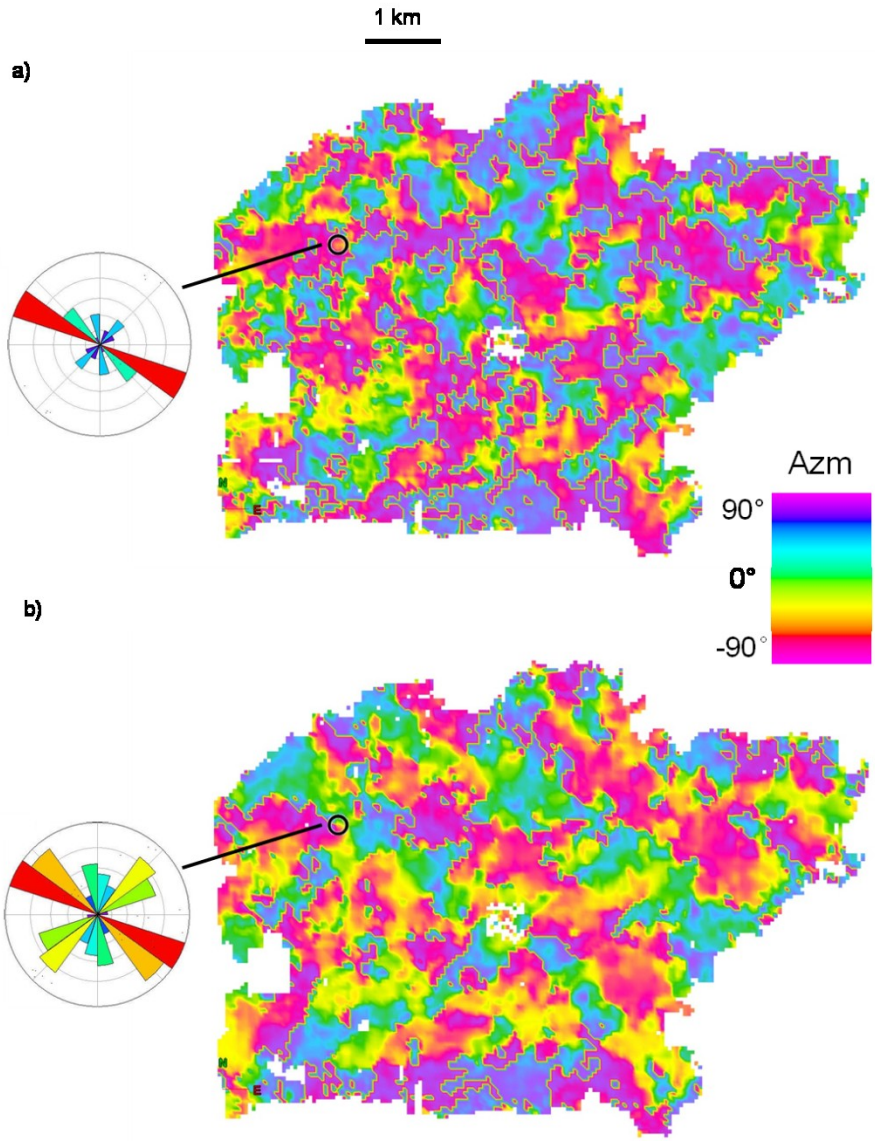

Figure 21. Maps showing the envelope weighted wavelet frequency azimuth of the ellipse fit for (a) Marble Falls and (b) Lower Barnett Shale. The rose diagrams show the interpreted fractures at the wellbore located inside the black circle on the azimuth maps. The azimuths of the fractures are shown above the Lower Barnett Shale (a) and below the Lower Barnett Shale (b). There is a high correlation with the amplitude azimuth and the interpreted fracture direction.

Several hundred micro-seismic experiments have been conducted in the Fort Worth Basin. Such experiments are commonly used to observe and map hydraulic fracture stimulations of reservoirs (Hunt et al., 2010). In addition to

observing and mapping a subset of the fractures due to the stimulation of the well, micro-seismic events can be used in conjunction with other seismic attributes to categorize wells and relate to production. Browning (2006), found that micro-seismic event locations occur more often in negative curvature zones, whether the well was drilled onto a positive curvature feature or into a negative curvature zone. Browning (2006) also observed that wells with more widely distributed micro-seismic events exhibited better production rates. Velocity anisotropy can also be used to predict micro-seismic event locations and production (Rich 2010). Low velocity anisotropy or alternatively anisotropy orthogonal to the regional maximum horizontal stress direction, combined with all of the previous characteristics further enhances the production of the well.

Figures 22a and 22b show a well that exhibits the same behavior described by Browning (2006), where the micro-seismic events follow velocity anisotropy and trend towards negative curvature. Figure 23 is a crossplot of most positive curvature extracted at all microseismic events versus event density (number of microseismic events). While there appears to be more events in positive values of most positive curvature, there are actually more events in zero or negative values. “Zero” is determined by the normal distribution of the most positive curvature, which is about 0.01 for this dataset.

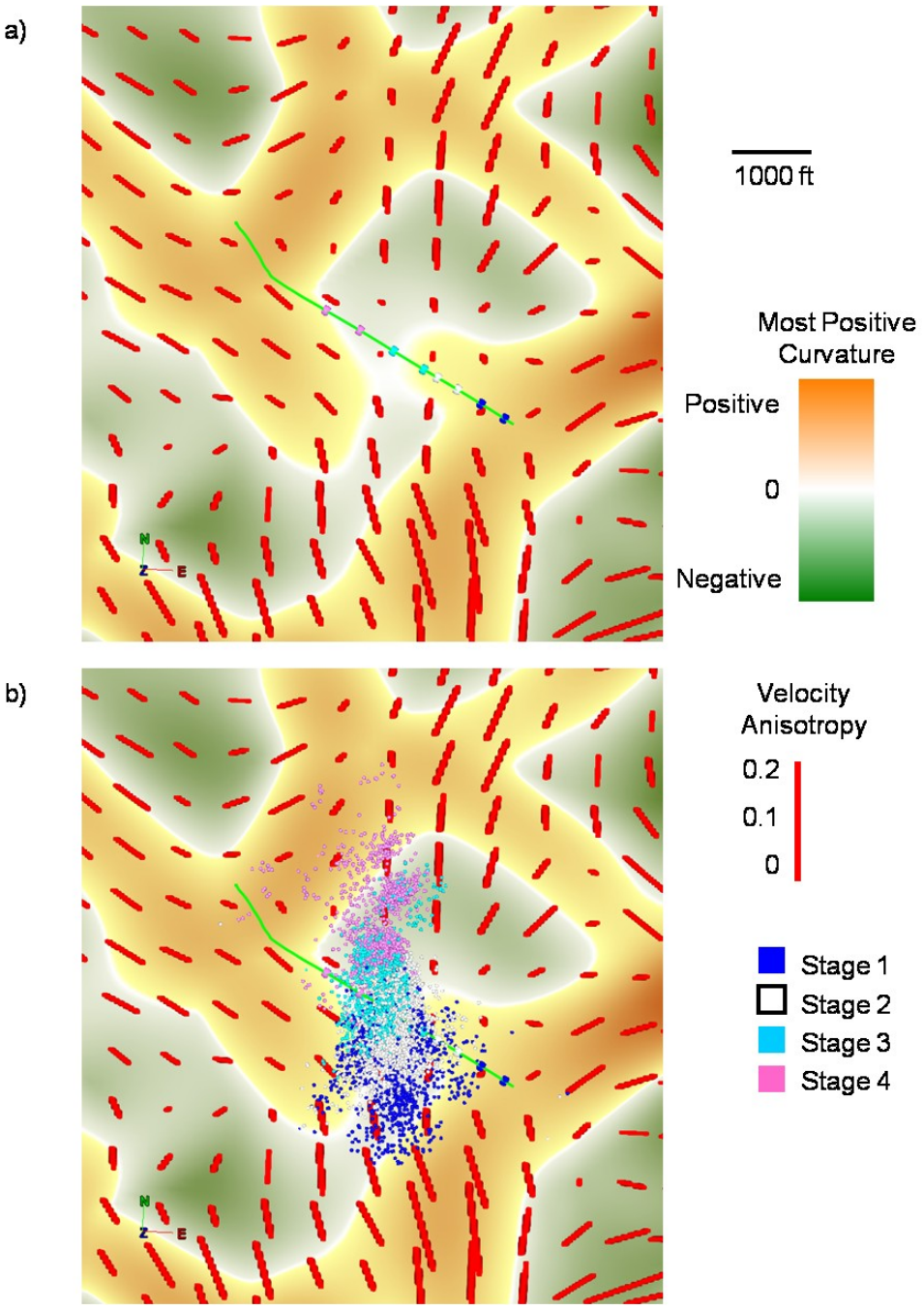

Figure 22. (a) Velocity anisotropy (red vectors) co-renedered with most positive curvature extracted along the top of the Viola. The length of the vector is proportional to the degree of anisotropy while the direction indicates the azimuth of maximum anisotropy. Notice the low magnitude velocity anisotropy near the wellbore and the N/S direction. Perforation zones are color-coded by their stage number. (b) Same image with micro-seismic events color-coded by stage number. Notice the micro-seismic events follow the anisotropy and exhibit a N/S trend, clustering in structurally low areas and preferring areas with negative values of curvature.

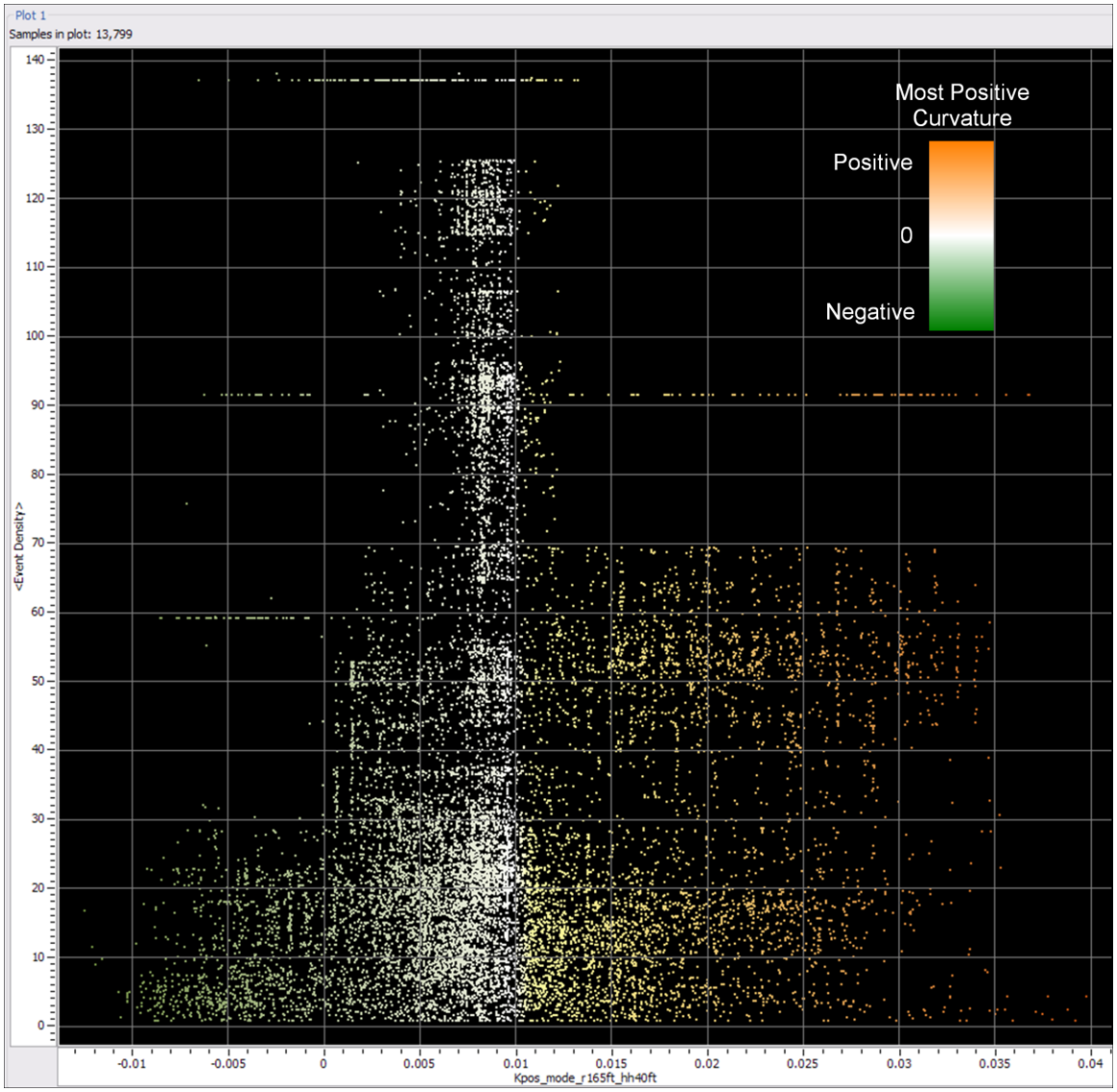

Figure 23. Crossplot of all wells' micro-seismic event density versus most positive curvature color-coded by most positive curvature. Unlike most positive curvature, the micro-seismic events do not occur in a normal distribution. Approximately two-thirds of the micro-seismic events occur in zero or negative values of most positive curvature.

Comparing the micro-seismic events with the ellipse fit eccentricities filtered by reliability I expected to see greater eccentricities where the micro-seismic events occurred. Surprisingly, I saw the opposite; the micro-seismic appeared in areas of low eccentricity and low reliability (Figures 24 and 25). This

suggests a complex fracture network resulted from the hydraulic stimulation of the well.

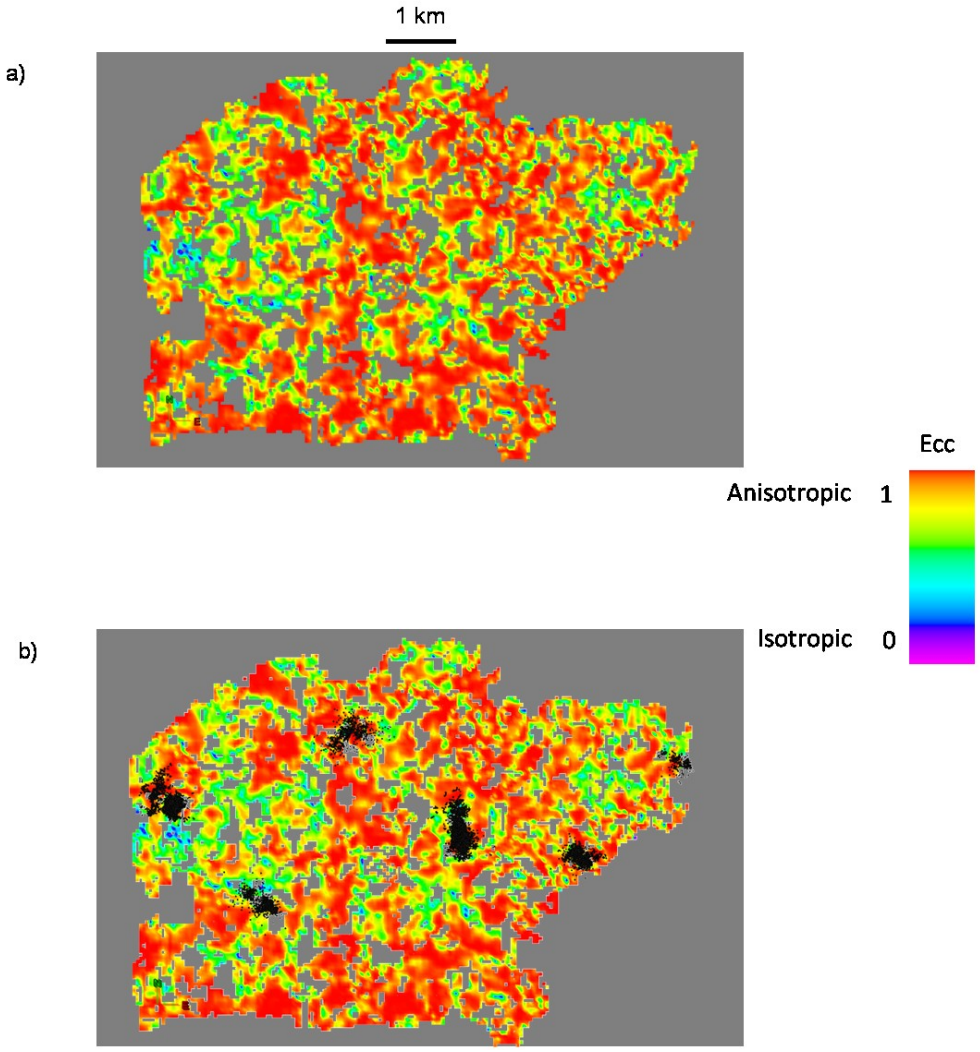

Figure 24. (a) Eccentricity, *e*, previously displayed in Figure 19, but rendered transparent when its reliability, *R*, given by equation B7 falls below an acceptable threshold. b) The same image showing the locations of events from six micro-seismic experiments. Notice the micro-seismic events appear in areas of low reliability and low eccentricity.

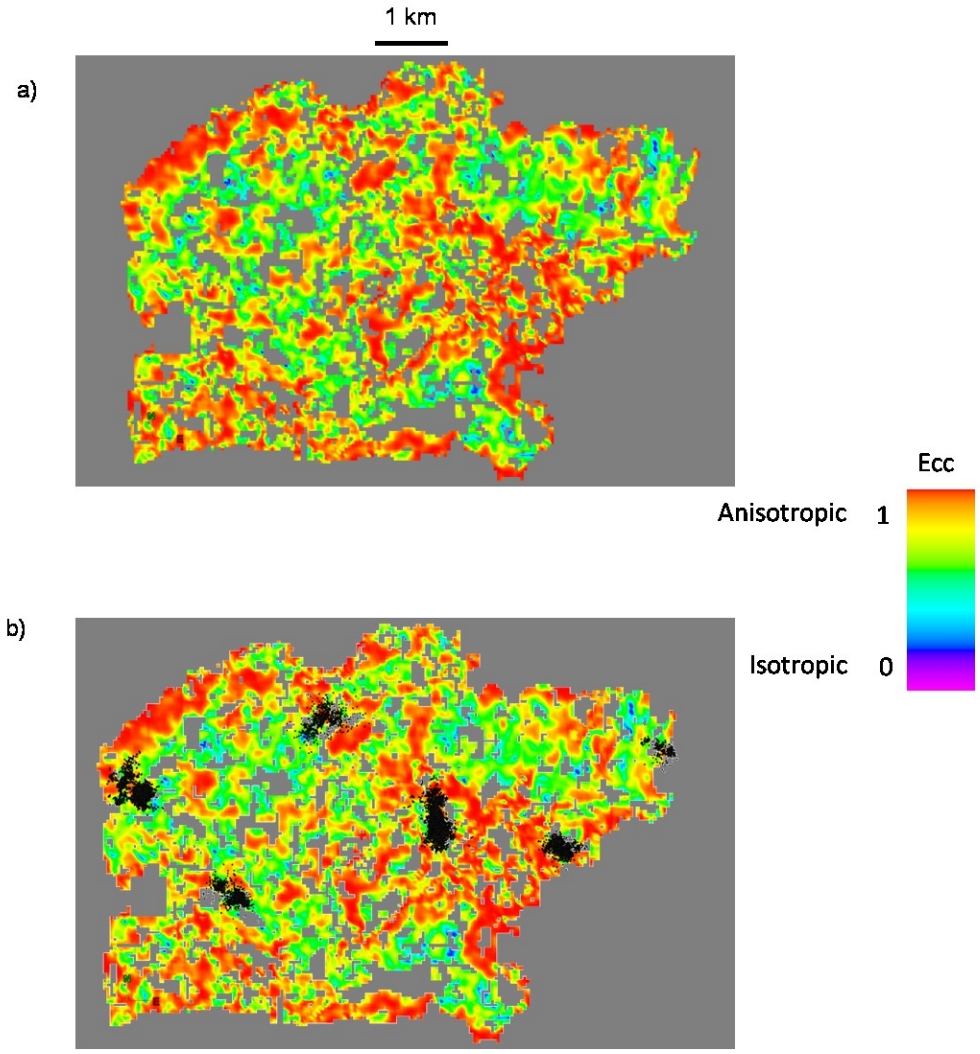

Figure 25. The same data as Figure 24, but now extracted along the Viola fracture barrier. The overall eccentricity is less than in the hydraulically-fractured Lower Barnett Shale.

The analysis of the micro-seismic data, that is available for most of the wells, not only has location and magnitude data available, but also the azimuth of the maximum horizontal stress, i.e., the direction in which the induced hydraulic fracture plane is oriented. To verify the findings of multiple azimuths within our producing zone, I made rose diagrams of the stress direction of the micro-seismic events and evaluated these along with the direction of the high contrast

zones (open conductive fractures) found on the image logs. The rose diagrams confirmed the finding of multiple azimuths from the mapping of eccentricities. The conclusion is that there are multiple fracture orientations in the subsurface created by hydraulic fracturing which creates an anisotropic symmetry that is more complex than the orthorhombic symmetry assumed at the beginning of the study.

Chapter 6

CONCLUSIONS AND LIMITATIONS

The findings of this study coincide with previous findings from the use of surface seismic and specialty log data in the Barnett Shale. The ellipse fitting of the attributes further verified that multiple azimuth directions are seen within the fractured interval and are more complex than recently thought. The most-positive curvature shows the history of deformation within the Fort Worth Basin and how it affects induced fractures. Velocity anisotropy can give details of present-day existing structural features and link these features and induced fractures to the curvature. Maximum horizontal stress for the basin is known to be northeast. While curvature, velocity anisotropy, and maximum horizontal stress all play a part in predicting how the induced fractures will behave, there is not one dominant azimuth the induced fractures prefer. This study has shown that where the wells have been hydraulically fractured there is a very complex fracture fairway that is created. It cannot be assumed there is orthorhombic symmetry within the fractured interval and therefore the areas of induced fractures cannot be mapped directly from P-wave surface seismic alone. The use of P-S data may be able to provide insights of areas of hydraulically-induced fractures with two or more sets of cracks.

As with any study there are short-comings of the data due to restrictions of cost, culture, and gross over-simplifications of the data. The restrictions due to cost and culture affect acquisition parameters and ultimately data quality. Minimizing costs does not affect the quality of the surface seismic as much as it

affects the data quality of the micro-seismic experiments. The micro-seismic experiments are conducted with only one monitor well, which adds significant error in the detection, location, and identification of the events. Cost does not play as large of role in affecting data quality as culture does for the surface seismic studies. The vast majority of seismic experiments collected in the Fort Worth Basin are termed to be 'urban seismic', meaning they are being conducted in peoples' back yards. This, along with the amount of pipelines, rigs and other industry-related culture significantly impacts where the shots are located and somewhat affects receiver locations. Cost also limits the type of seismic experiments that are conducted. Ideally, time lapse and true P-S seismic experiments would be conducted to acquire more detailed information of induced fracture location and density.

Simplifications in the data can also be hazardous to any type of study. The complex completion histories in this area are unable to be fully accounted for, so simplifying the production data will inherently create errors in results. Production from shale gas is relatively new in the industry and is still not well understood. By making assumptions as to how wells are producing and by simplifying the fracture extents and orientations, and by not using production logs in horizontal wells to measure production from each stage so it can better be correlated to seismic attributes, there becomes more error in results, but most importantly, prevents an open-minded approach to a very complex system, which magnifies the problems.

REFERENCES

Appleton, G. J., 2010, Personal correspondence: Devon Energy.

Ammerman, M.L.,2010, Personal correspondence: Devon Energy.

Barnes, A. E., 2000a, Weighted average seismic attributes: Geophysics, **65**, 275–285.

Browning, D. B., 2006, Investigating correlations between microseismic event data, seismic curvature, velocity anisotropy, and well production in the Barnett Shale, Fort Worth Basin, Texas. Master's Thesis, The University of Oklahoma, Norman.

Goodway, B., 2007, Isotropic AVO methods to detect fracture prone zones in tight gas resource plays: CSPG CSEG Expanded Abstracts, 585-589.

Goodway, B., 2007, Anisotropic 3D amplitude variation with azimuth (AVAz) methods to detect fracture prone zones in tight gas resource plays: CSPG CSEG Expanded Abstracts, 590-596.

Hale-Elrich, W.S., and J.L. Coleman Jr., 1993, Ouachita-Appalachian Juncture: a Paleozoic Transpressional Zone in the Southeastern U.S.A.: The American Association of Petroleum Geologists Bulletin, **77**, 552-568.

Erlich, R.N., and J. L. Coleman Jr., 2005, Drowning of the Upper Marble Falls carbonate platform (Pennsylvanian), central Texas: A case of conflicting "signals?": Sedimentary Geology, **175**, 479-499.

Grechka, V. and I. Tsvankin, 1998, 3-D description of normal moveout in anisotropic inhomogeneous media: Geophysics, **639**, 1079-1092.

Groundwater Protection Council, 2009, Modern Shale Gas Development in the United States: A Primer, http://www.gwpc.org/e-library/documents/general/Shale%20Gas%20Primer%202009.pdf, Accessed 20 May 2010.

Hunt, L., S. Reynolds, T. Brown, S. Hadley, J. Downton, and S. Chopra, 2010a, Am I really predicting natural fractures in the tight Nordegg Gas Sandstone of west central Alberta? Part I: Theory and statistics: GeoCanada 2010 Conference, http://www.geocanada2010.ca/program/program-schedule/tuesday/pm-2/seismic-interpretation-case-studies.html, Accessed 10 Aug 2010.

Hunt, L., S. Reynolds, T. Brown, S. Hadley, J. Downton, and S. Chopra, 2010b, Am I really predicting natural fractures in the tight Nordegg Gas Sandstone of west central Alberta? Part II: Observations and conclusions: GeoCanada 2010 Conference, http://www.geocanada2010.ca/program/program-schedule/tuesday/pm-2/seismic-interpretation-case-studies.html, Accessed 10 Aug 2010.

Kalkomey, C. T., 1997, Potential risks when using seismic attributes as predictors of reservoir properties: The Leading Edge, **16**, 247-251.

Janwadkar, S., S. Morris, M. Potts, J. Kelley, D. Fortenberry, G. Roberts, M. Kramer, S. Privott, and T. Rogers, 2007, Advanced LWD and directional drilling technologies overcome drilling and completion challenges in lateral wells of Barnett Shale: SPE 110837.

Lafollette, S.G., 2009, Personal correspondence: Devon Energy.

Lynn, H., 2004, The winds of change Anisotropic rocks-their preferred direction of fluid flow and their associated seismic signatures-Part 1, The Leading Edge, **23**, 1156-1162.

Lynn, H., 2010, Personal correspondence: Lynn Inc.

Morlet, J., G. Arens, E. Fourgeau, and D. Giard, 1982, Wave propagation and sampling theory – Part II: Sampling theory and complex waves: Geophysics, **47**, 222-236.

Narhari, S. R., A. L. Al-Kandari, V. K. Kidambi, S. Al-Ashwak, B. Al-Qadeeri, and C. Pattnaik, 2009, Understanding fractures through seismic data: North Kuwait case study: The 79th Annual International Meeting of the SEG, Expanded Abstracts, 547-551.

Perez, R., 2009, Quantitative petrophysical characterization of the Barnett Shale in the Newark East Field, Fort Worth Basin. Master's Thesis, The University of Oklahoma, Norman.

Polastro, R. M., D. M. Jarvie, R. J. Hill, and C. W. Adams, 2007, Geologic framework of the Mississippian Barnett Shale, Barnett-Paleozoic total petroleum system, Bend arch-Fort Worth Basin, Texas: AAPG Bulletin, **91**, 405-436.

Quinn, T.H., J. Dwyer, C. Wolfe, S. Morris, and D. Coope, 2008, Formation evaluation logging while drilling (LWD) in unconventional reservoirs for production optimization: SPE 119227.

Refunjol, X. E., K. M. Keranen, and K. J. Marfurt, 2010, Inversion and attribute-assisted hydraulically-induced microseismic fracture prediction: A North

Texas Barnett Shale case study: 80th Annual International Meeting of the SEG, Expanded Abstracts

Rich, J.P., and M. Ammerman, 2010, Unconventional geophysics for unconventional plays: SPE 131779.

Roende, H., C. Meeder, J. Allen, S. Peterson, D. Eubanks, and C. Ribeiro, 2007, Estimating subsurface stress direction and intensity from surface full azimuth land data: 77th Annual International Meeting of the SEG, Expanded Abstracts, 217-220.

Roth, M., and A. Thompson, 2009, Fracture interpretation in the Barnett Shale using macro and micro-seismic data: First Break, **27**, 61-66.

Simon, Y. S., 2005, Stress and fracture characterization in a shale reservoir, North Texas, using correlation between new seismic attributes and well data: M.S. Thesis, The University of Houston.

Singh, S., H. Abu-Habbiel, B. Khan, M. Akbar, A. Etchecopar, and B. Montaron, 2008, Mapping fracture corridors in naturally fractured reservoirs: an example from Middle East carbonates: First Break, **26**, 109-113.

Schlumberger, 2010, The Oilfield Glossary: Where the Oil Field Meets the Dictionary, http://www.glossary.oilfield.slb.com/, Accessed 20 Sept 2010.

Taner, M. T., 2000, Attributes revisited: http://www.rocksolidimages.com/pdf/attrib_revisited.htm, Accessed 29 Dec 2009.

Taner, M. T., F. Koehler, and R. Sheriff, 1979, Complex seismic trace analysis: Geophysics, **44**, 1041-1063.

Thompson, A., J. Rich, and M. Ammerman, 2010, Fracture characterization through the use of azimuthally sectored attribute volumes: 80th Annual International Meeting of the SEG, Expanded Abstracts.

Widess, M. B., 1973, How thin is a thin bed?: Geophysics, **38**, 1176-1254.

Zhang, K., B. Zhang, J. T. Kwiatkowski, and K. Marfurt, 2010, Seismic azimuthal impedance anisotropy in the Barnett Shale: 80th Annual International Meeting of the SEG, Expanded Abstracts.

APPENDIX A: SEISMIC DATA QUALITY

In April 2009, Devon Energy acquired a wide azimuth 51 km^2 proprietary 3D seismic data over the study area. A smaller three-component survey overlaps 14.5 km^2 of the P-wave survey. Overall, the P-wave seismic data are high quality (Figure 6), with frequencies approaching 100 Hz. Table A-1 summarizes the acquisition parameters.

Table A-1: Acquisition parameters used to allow subsequent azimuthal processing

Number of live lines:	30
Number of stations per line:	120
Receiver line interval	660 ft (201 m)
Receiver group spacing	220 ft (67 m)
Shot line interval	880 ft (268 m)
Vibrator array interval	220 ft (67 m)
Patch size	26,180 ft by 25,520 ft (7,980m by 7,778m)
Nominal bin size	110 ft by 110 ft (33 m by 33 m)
Number of vibrator sweeps	8
Number of vibrators per array	3
Sweep range	10-110 Hz, 10 s duration, 3 db/octave
Number of geophones per group	6 in a 6 ft (2 m) circle around station

Figure A-1 shows the fold of the entire survey while Figure A-2 shows the azimuths (displayed as spider diagrams) of the midpoints inside the highlighted red square shown in Figure A-1.

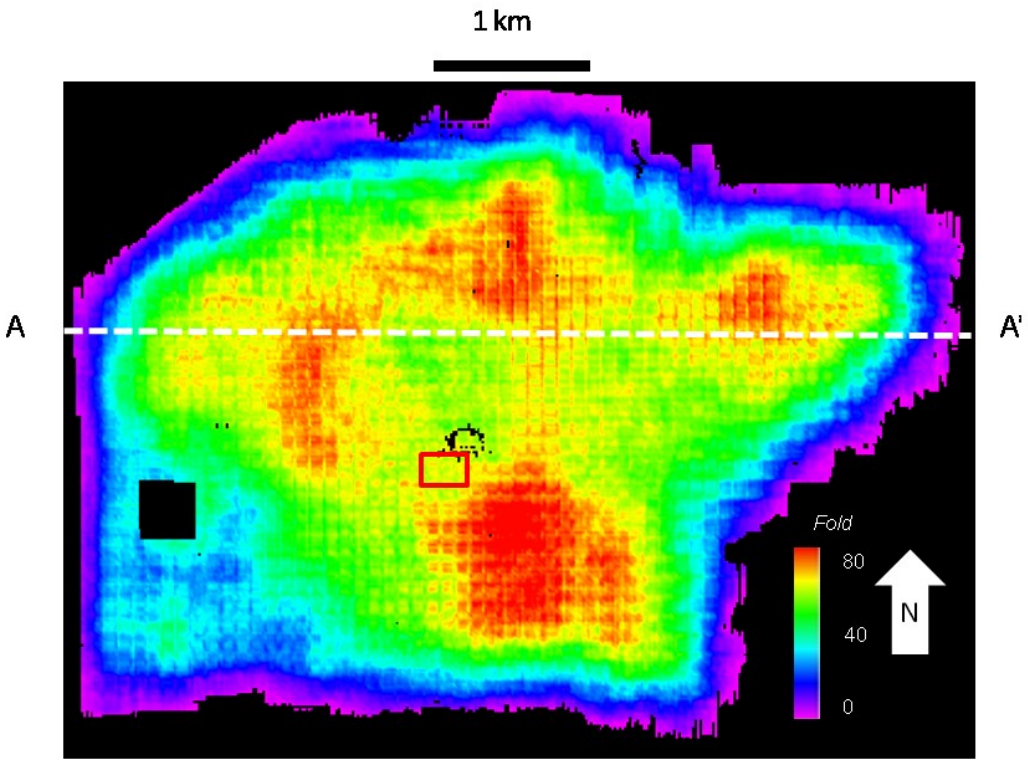

Figure A-1. Fold of angle stacks 0-35 degrees along the top of the Viola limestone horizon. Line AA' is displayed in Figure 3. Spider diagrams that fall within the red square are shown if Figure A-2.

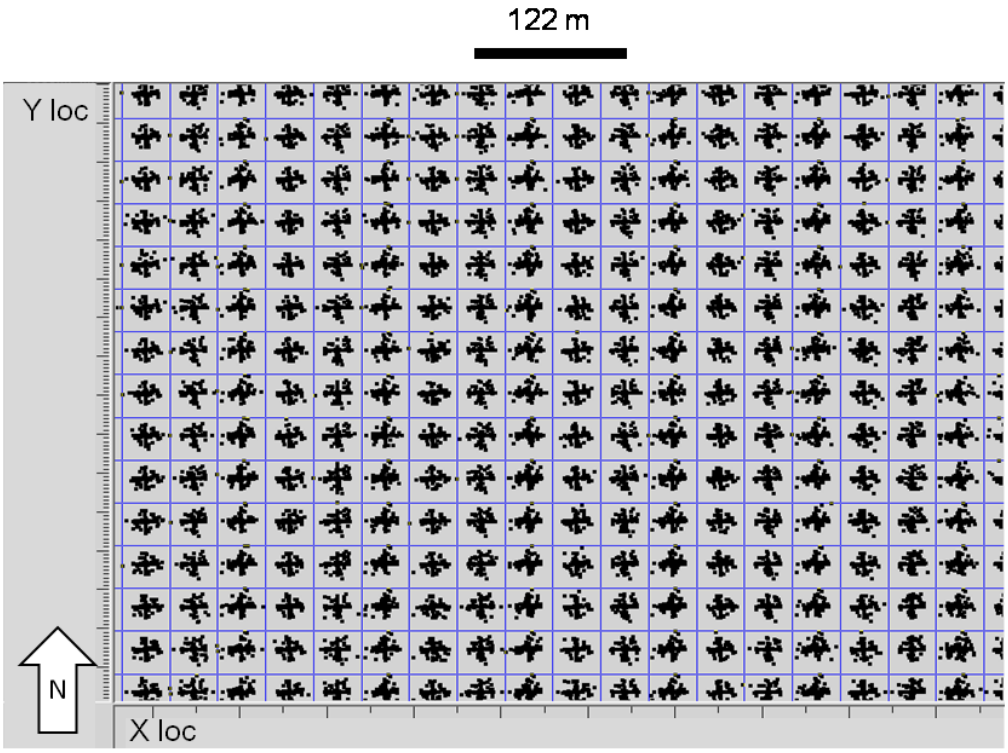

Figure A-2. Spider diagram of the azimuthal coverage corresponding to the CMP bins displayed in the red box shown in Figure A-1. Note the azimuthal coverage is wide, and close to uniform.

In addition to the seismic amplitude volume, other products include several state-of-the-art commercially-generated volumes with angle stacks, sectored-azimuth stacks, P-wave velocity anisotropy analysis, and azimuthal AVAz volumes that are used in conjunction with post-stack volumetric attributes.

The individual azimuth volumes had consistent amplitudes from trace to trace, so each trace was multiplied by 1100 to bring the amplitudes to a range of +/- 25,000. The processing sequence for the azimuthal sectored volumes began with spherical divergence correction; air blast attenuation, surface consistent amplitude correction, and narrow band anomolous amplitude noise reduction. Followed by surface consistent deconvolution, refraction statics solution and

application. There was two iterations of velocity analysis and residual statics. Next there was imaging velocity analysis applied. The data was re-binned to 220 ft by 220 ft bins; pre-stack time migration to offset vector tile space (OVT). The processor applied AZIM(tm), azimuthal velocity analysis/application to every third common depth point (CDP). A stack mute as well as trim statics was applied (max shift=10 ms). Automatic Gain Control (AGC) was applied in a one second median, CDP stack, and time variant filter (interpolation between control points) 0.0-1.0 sec: 10/15-90/110 Hz; 1.4 sec: 10/15-80/100 Hz; 1.8 sec: 10/15- 75/95 Hz; 2.2-3.0 sec: 10/15- 45/58 Hz.

Due to the scaling for the amplitude values, care should be taken when using these data for analysis. Surgical mutes were also applied to the top and bottom of traces to deal with erroneously high values that could cause unrealistic results in any attribute calculation.

Within this survey there are 435 Devon-operated Barnett gas wells, of which 384 wells are vertical or directional wells and 164 are horizontal wells. In terms of special processes, image logs were run on sixteen wells before April 2009, two wells after April, 2009, while micro-seismic experiments were run on fifteen wells.

In addition to these specialty log experiments, two wells contain production logs, four wells have conventional (whole) cores, eight wells have sidewall cores and one well has both conventional and sidewall cores. Completions for vertical wells are within the Upper and Lower Barnett interval and horizontal wells are primarily landed and completed in the Lower Barnett

interval; however, there are seven horizontal Upper Barnett completions including one well with micro-seismic measurements.

APPENDIX B: AMPITUDE VERSUS AZIMUTH

Gretchka and Tsvankin (1998) showed how the NMO velocity in a medium with horizontally transverse symmetry can be fit by an ellipse. Fitting such an ellipse to time delays in azimuthally-sectored data is the standard approach to azimuthal velocity analysis. Our goal here is to exploit the azimuthal variations in waveform, independent of the more common time shifts or amplitude variation with azimuth (AVAz). In order to avoid the overprint of the time-delay anisotropy, the same horizon is interpreted on each of the azimuthally-sectored volumes. Phantom horizons parallel to the picked horizon are then used to extract a given attribute for each corresponding azimuthally-sectored volume. These attribute values, $A(\theta)$, are then fit to an ellipse using the methodology of Thompson et al. (2010):

$$A(\theta) = a\cos^2\theta + b\cos\theta\sin\theta + c\sin^2\theta, \tag{B1}$$

by casting equation B1 for each azimuth, θ_j, in matrix form

$$\begin{pmatrix} \cos^2\theta_1 & \cos\theta_1\sin\theta_1 & \sin^2\theta_1 \\ \cos^2\theta_2 & \cos\theta_2\sin\theta_2 & \sin^2\theta_2 \\ \dots & \dots & \dots \\ \cos^2\theta_n & \cos\theta_n\sin\theta_n & \sin^2\theta_n \end{pmatrix} \begin{pmatrix} a \\ b \\ c \end{pmatrix} = \begin{pmatrix} A_1 \\ A_2 \\ \dots \\ A_n \end{pmatrix}. \tag{B2}$$

Equation B2 has the form **A=TC**, where the vector **A** contains the measured attributes, the vector **C** the unknown coefficients, and **T** is a matrix of the sines and cosines evaluated at the measurement azimuths, θ_j. Equation B2 can be solved using least-squares:

(B3)

where I is the identity matrix and σ a small positive number used to stabilize the result. In order to find the major and minor axes of the ellipse, we rotate the ellipse by some angle β such that these line up with the local coordinate system. For our problem, the equation of the ellipse can be written as

$$A(\theta_j) = \lambda_1 \cos^2(\theta_j - \beta) + \lambda_2 \sin^2(\theta_j - \beta) , \quad \text{(B4)}$$

where λ_1 and λ_2, are the eigenvalues of the matrix formed by the general coefficients (Figure B-1)

$$\begin{pmatrix} a & b \\ b & c \end{pmatrix} \quad \text{(B5)}$$

and where β is the azimuth of the eigenvector associated with the eigenvalue λ_1. The eccentricity, e, (or degree of anisotropy) of the best-fit ellipse is given by

$$e = \sqrt{1 - \left(\frac{\lambda_2}{\lambda_1}\right)^2} . \quad \text{(B6)}$$

Since by construction, $\lambda_2 \leq \lambda_1$, $0 \leq e \leq 1$. The reliability of the azimuthal attribute is defined as

. (B7)

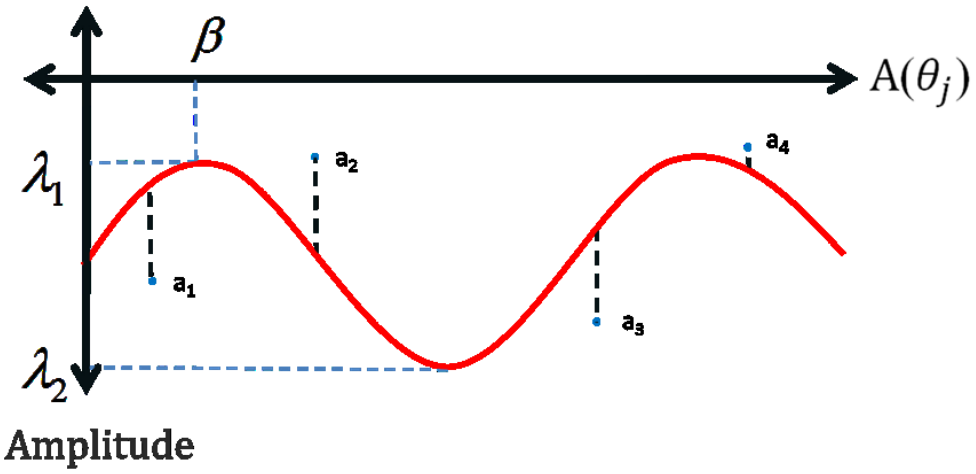

Figure B-1. Diagram showing the fit of an ellipse having the form of equation B4 to attribute measures a_j made at four different azimuths, θ_j. The eccentricity, e, shown in Figure 9 is a function of λ_1 / λ_2. The reliability, R, shown in Figure 10 is a measure of the distance between the blue circles and the red curve.

APPENDIX C: GLOSSARY

The following technical words used in this paper are commonly used in the production of shale gas.

Bashing – During a hydraulic fracture job, injected fluid travels to a neighboring well typically negatively impacting its production. Also called 'depletion' by many operators. It's acceptable (but not good) to bash your own well, but it is not acceptable to bash someone else's well.

Breakdown Pressure – Amount of pressure needed to achieve fractures in the reservoir rock by the injected fluid.

Damage Zone – Area of hydraulically induced fracturing that is open and flowing fluid to the wellbore.

EUR – Expected ultimate recovery of a well. Represents the amount of gas the well is expected to produce over its lifetime.

Frac – see Hydraulically-Induced Fracture.

Fracability – The ability of the rock to be hydraulically fractured.

Hydraulically-Induced Fracture - A stimulation treatment routinely performed on oil and gas wells in low-permeability reservoirs. Specially engineered fluids are pumped at high pressure and rate into the reservoir interval to be treated, causing a vertical fracture to open. The wings of the fracture extend away from the wellbore in opposing directions according to the natural stresses within the formation. Proppant, such as grains of sand of a particular size, is mixed with the treatment fluid to keep the fracture open when the treatment is complete. Hydraulic fracturing creates high-conductivity communication with a large area of

formation and bypasses any damage that may exist in the near-wellbore area (Schlumberger 2010).

Pump Curve – During hydraulic fracture treatment treating pressures, wellhead rates, calculated bottomhole pressures, wellhead and bottomhole proppant concentrations, slurry flow rates, slurry proppant concentrations and the direction of the job are recorded and plotted on the pump curve. The pump curve shows how the frac job has progressed through time and can show the breakdown of the rock (Schlumberger 2010).

Micro-seismic (Hydraulic Fracture Monitoring) - A technique to track the propagation of a hydraulic fracture as it advances through a formation. Microseisms are detected, located, and displayed in time for scientists and engineers to approximate the location and propagation of the hydraulic fracture. Also known as micro-seismic monitoring, this technique delivers information about the effectiveness of the stimulation of a reservoir that can be used to enhance reservoir development in shale gas completions (Schlumberger 2010).

Refrac - An operation to restimulate a well after an initial period of production. Refracturing operations attempt to bypass near-wellbore damage, reestablish good connectivity with the reservoir, and tap portions of the reservoir with higher pore pressure. Refracturing operations are also performed after a period of production that can alter the stresses in a reservoir due to depletion; the re-stimulation can allow the new fracture to reorient along a different azimuth. A successful refracturing operation may restore well productivity to near original or

even higher rates of production and extends the productive life of a well (Schlumberger 2010).

Slick Water – Friction-reduced water containing polyacrilimide (liquid plastic) used to hydraulically fracture the reservoir.

Stimulate - A treatment performed to restore or enhance the productivity of a well. Stimulation treatments fall into two main groups: hydraulic fracturing treatments and matrix treatments. Fracturing treatments are performed above the fracture pressure of the reservoir formation and create a highly conductive flow path between the reservoir and the wellbore. Matrix treatments are performed below the reservoir fracture pressure and generally are designed to restore the natural permeability of the reservoir following damage to the near-wellbore area. Stimulation in shale gas reservoirs typically takes the form of hydraulic fracturing treatments (Schlumberger 2010).

APPENDIX D: ATTRIBUTE DEFINITIONS

Commercial software and technology service providers often use different names for the same attributes. In this appendix, I define the mathematical basis and/or definition of the attributes that I have evaluated. Good references include Tanner (1979) and (2000), Barnes (2000), and Morlet (1982).

Gabor-Morlet Spectral Components - The component of the seismic data that can be represented by a wavelet constructed by windowing a cosine waveform at frequency, *f*, temporarily windowed by a Gaussian whose standard deviation defines the wavelet bandwidth.

Gabor-Morlet Spectral Magnitude – The magnitude (or alternatively, the envelope) of a given Gabor-Morlet spectral component, at time, *t*.

Gabor-Morlet Spectral Phase – The phase of a given Gabor-Morlet spectral component at time, *t*.

Gabor-Morlet Spectral Trace – The trace of a given Gabor-Morlet spectral component at time, *t*.

Gabor-Morlet Mean Frequency – The mean frequency of the spectral components obtained using Gabor-Morlet spectral decomposition.

Gabor-Morlet Q Frequency Shift – An estimation of attenuation, 1/Q, obtained by computing the frequency shift of the Gabor-Morlet spectral decomposition components.

Gabor-Morlet RMS Frequency – Root-mean-square frequency of the spectra obtained using Gabor-Morlet spectral decomposition.

SOF Amplitude – Structure-oriented filtered version of the seismic amplitude. Filters are applied in a small analysis window aligned with dip and azimuth, can be edge-preserving, and include, mean, alpha-trimmed mean, and principal-component filters.

TWT– Value of a picked seismic event (e.g. two-way travel time of a peak, trough, or zero-crossing)

Analytic trace – The complex-valued time series obtained by forming a complex time series constructed by combining the measured seismic amplitude (the real component) and its Hilbert transform (the imaginary component).

Imaginary Component – Imaginary part of the analytic trace. Alternatively called the Hilbert transform or quadrature of the "real" or measured seismic amplitude.

Real Component – Real part of the analytic trace which is the measured seismic amplitude.

Envelope Derivative – Time derivative of the envelope of the analytic trace, time rate of change of envelope. Envelope derivatives computed at the onset of an event may indicate absorption effects, with smoother increases indicating larger absorption and sharper increases implying a wider bandwidth and less absorption.

Mean Frequency – Envelope-weighted instantaneous frequency obtain by computing the weighted average of the instantaneous frequency within a vertical analysis window where the weights are the corresponding envelope values. This estimate suppresses artifacts in the instantaneous

frequency associated with waveform interference that occurs at envelope minima. Typical window sizes range between 5 and 11 samples.

Acoustic Impedance – Relative acoustic impedance computed by integrating the trace followed by a low-pass filter.

Wavelet Envelope Derivative – A blocked version of the time derivative of the envelope evaluated at the envelope peak that is then assigned to all sample between adjacent envelope minima.

Wavelet Attributes – Attributes representing the seismic wavelet rather than a given sample in a two step process: First, the envelope is computed. Then, the attribute is evaluated at local envelope maxima and assigned to all values between the adjacent local envelope minima. Also called the Response Attribute.

Wavelet Dominant Frequency – The envelope-weighted mean frequency evaluated at the nearest envelope maxima. (See wavelet attribute)